Photoluminescence studies of radioactive mercury and gold impurity centres in silicon

James Fryar

M.Sc. Thesis **2001**

Photoluminescence studies of radioactive mercury and gold impurity centres in silicon

Dissertation for the award of Master of Science

By

James Fryar, B.Sc.

September 2001

Prof. M. O. Henry
Semiconductor Spectroscopy Laboratory
School of Physical Sciences
Dublin City University

Declaration

I hereby certify that this material, which I now submit for assessment on the programme of study leading to the award of Master of Science, is entirely my own work and has not been taken from the work of others save and to the extent that such work has been cited and acknowledged within the text of my work.

Signed: _____ ID No.: _____

Acknowledgements

I would like to express my heartfelt thanks to Prof. M. O. Henry for his encouragement and enthusiasm in guiding me through the research presented here, and for accepting me to this group. Had it not been for his level of dedication, and his extensive knowledge and experience, this thesis would not have been possible.

I am indebted to Dr. E. McGlynn, whose continuous help with regard to maintaining equipment, analysis of results obtained and general unwavering support, have enabled me to complete this research. His energy and dedication to this field are enviable, and I thank him for always finding the time to answer my queries.

I would like to acknowledge the support of Dr. M. Dietrich, Dr. J. Bollmann, and Mr. R. Ludwig during the implantation of samples at ISOLDE. Without their extensive help, few of the measurements presented here would have been possible. Thanks to them, the ISOLDE equipment is not quite as intimidating as it once appeared!

Finally, I would like to dedicate this thesis to my parents. To my mother I am grateful for her continuous support and love throughout my years, and for sacrificing so much to allow me to follow this path. I thank my father for instilling in me a love of physics and the natural world, and I hope this thesis is a worthy tribute to his guidance and love.

Abstract

The implantation of radioactive isotopes into semiconductor materials is a powerful technique that enables researchers to correctly assign chemical identities to defects observed by spectroscopic methods. Since each radioactive isotope has a characteristic decay rate, the intensity of spectroscopic features related to those atoms should also change with a corresponding rate, allowing an accurate identification of defect centres.

This report shall discuss a number of Hg- and Au-related defects in silicon studied by Photoluminescence Spectroscopy. Radioactive ^{197}Hg decays to stable Au, enabling defects involving both elements to be studied. Data presented here, based on implantations of ^{197}Hg and stable ^{200}Hg, confirms a previously observed Hg-related feature. It contains three Zero Phonon Lines and is due, we believe, to a three-level ground state and double excited states for the Hg atoms. The 'FeB' defect centre, previously shown to involve Au, is also studied. Whilst confirmation of the involvement of Au could not be established, an analysis has shown that thermal dissociation of this defect may negatively influence the results of spectroscopic measurements. A defect probably involving Au and Li is also studied, illustrating the techniques necessary to produce it. Again, this defect appears to dissociate upon room temperature storage at a rate similar to the 'FeB' defect, suggesting that Au is involved in this process for each.

Finally, the results of an examination of Si:Ge Multi-Quantum Well (MQW) structures are presented. These indicate that much of the luminescence observed is related to either bulk- or surface-related dislocations in the Si rather than the quantum structures themselves.

Section 1: Introduction

1.1 Semiconductor Materials

In 1947 Bardeen, Brattain, and Shockley developed the world's first transistor, all three later winning the Nobel Prize for their research. From that moment onwards the semiconductor industry began to blossom. Digital electronics meant smaller, cheaper, and more reliable calculating machines and with the US and USSR beginning to turn their sights on launching military, research and manned rockets into space, development of computers and digital electronics relating to these applications was rapid. New semiconductor-based calculators allowed for more accurate modelling of gravitational forces, and the angles and speeds required for safe re-entry of vehicles into the atmosphere, as well as enabling manoeuvres, rocket burns and navigation to be electronically controlled. Although not the sole beneficiary or raison d'être of the new technology, the Space Race and Cold War were certainly major factors in the frantic pace of development, the large spending allocated to research, and the drive towards miniaturisation. Fragile glass valves were replaced by the smaller transistor, which also began a revolution in low-cost radio transmission and detection equipment. As the physical scale of these solid-state devices decreased, the first integrated circuits were developed. Today, every device requiring electronic control, from washing machines to fuel-injection systems in cars, is likely to have a 'chip' at its heart. In terms of profits, the electronics industry is second only to the massive oil producing companies.

Semiconductors are used for the manufacturing of microelectronics because their properties can be altered significantly by the introduction of impurity atoms to the crystal. These impurities alter the local number of charge carriers and introduce energy levels within the bandgap, thereby changing the electrical and optical characteristics of the crystal. In solid-state physics, terms such as 'impurity' or 'dopant' can be misinterpreted or carry certain unhelpful connotations. The word 'impurity', for example, is often applied to those unwanted atoms that have been accidentally added to crystals during growth, annealing or handling processes, whilst 'dopant' refers to atoms deliberately introduced. Sometimes the words are used interchangeably to simply mean any additional atoms or molecules found within the crystal structure. These semantics are not helpful in discussing the properties of semiconductor materials because they can give a false impression of the origin of the atoms found within the lattice. Experimenters use the general term 'defect', which is

any atomic or molecular contaminant in, or native lattice distortion of the intrinsic semiconductor material, regardless of its origin.

Approximately 90% of the world's electronic components and integrated circuits are manufactured using silicon. Silicon is relatively cheap to obtain and easy to grow with sufficient purity for the construction of devices. The effect of a wide range of defects in silicon has been an active field of research since the 1950s. This report shall discuss the impact and influence of certain mercury (Hg)- and gold (Au)-related defects in silicon, and the use of radioactive isotopes to make determinations of the chemical identity of defects.

1.2 Defects in Silicon

Silicon used for spectroscopic measurements generally contains many defects that are introduced during crystal growth and processing. Commercial Czochralski (CZ) grown silicon is oxygen rich, containing about 10^{17} atoms cm^{-3}. Float-zone (FZ) silicon, by comparison, typically contains at least an order of magnitude fewer oxygen atoms than this figure. The large concentration of oxygen within CZ silicon is due to the dissolution of the silica crucible in which the melt is held.

Oxygen atoms sit in interstitial sites, preferentially bonded to two neighbouring silicon atoms. This creates stacking faults in the crystal lattice, which helps prevent the extension of dislocations. The addition of oxygen therefore increases the strength of wafers, and its presence in high quantities is essential for producing VLSI electronic devices. Some applications in this field require concentrations as high as 10^{18} atoms cm^{-3}. A detailed analysis of oxygen in silicon is given by Bender and Vanhellemont[1].

Carbon is also found in silicon, present as a grown-in impurity and/or introduced during processing. Concentrations of 10^{16} atoms cm^{-3} are typical for CZ silicon, spanning about an order of magnitude less for FZ material. Carbon atoms introduced during the growth process have a tendency to occupy substitutional sites[2]. However, Reactive Ion Etching (RIE) is used in the manufacturing of sub-micron microelectronic devices, and carbon-tetrafluoride (CH_4) plasmas are routinely employed. Analysis has shown that carbon can be driven in from the CH_4 plasmas, and occupy interstitial sites within the silicon[3].

As well as these two elements, commercially produced silicon includes defects whose identity depends on the desired majority-carrier characteristics. In the case of p-type silicon, boron and aluminium are widely used to create acceptor energy levels just above the valence band. It should be noted that as well as oxygen, the melt used for CZ growth techniques can contain boron as an impurity from the silica crucible. For n-type doping, phosphorus and arsenic donors are commonly used. Although the number of acceptor or donor defects introduced will depend on the possible applications of the silicon, typical concentrations are between 10^{14} and 10^{17} atoms cm^{-3}.

Both interstitial carbon and oxygen are quite mobile at temperatures used for annealing. Carbon is known to form many complexes, for example, with another carbon atom[4], oxygen[5], and Group III acceptors such as boron, indium and aluminium[6,7]. Oxygen also forms complexes with aluminium[8] and other metals introduced into the crystal, including beryllium[9], zinc[10], and cadmium[11]. Copper is routinely found in appreciable quantities in silicon samples as a result of the use of heating elements during processing and annealing.

The electronic energy states produced by defects can be broadly divided into two categories. Energy levels close to the valence or conduction band are known as *shallow levels*, whilst any other level within the bandgap is known as a *deep level*. Shallow levels lie, typically, within a few tens of meV from the valence or conduction band edge. The defects responsible produce Coulombic forces or cause lattice strains which attract electrons or holes to the defect. Since these charge carriers will be loosely bound, their wavefunctions extend beyond neighbouring atoms. In contrast, deep level defects attract carriers and bind them tightly, the wavefunctions becoming highly localised. The energy of deep levels is therefore largely dependent on the chemical bonding of the defect atom to the surrounding lattice.

1.3 Spectroscopic Methods and the use of Radioactive Isotopes

There is a wide range of techniques available to the modern researcher for investigation of defects in semiconductor materials. Perhaps the most powerful is Deep Level Transient Spectroscopy (DLTS). DLT spectroscopy involves the creation of contacts on the semiconductor surface, and the application of pulses of either bias voltages or of light to the material. This excitation causes the filling of deep defect levels with charge carriers, followed by subsequent relaxation to thermal equilibrium. By obtaining current or capacitance measurements over a range of temperatures and pulse times, information pertaining to defect capture coefficients, activation energies and carrier mobility can be determined. DLTS is extremely useful because the depth of probing can be altered by changing the applied bias voltage, enabling the technique to distinguish between bulk crystal and surface defects. Clearly there is the possibility that copper from heating elements, aluminium or other metals from holders, or atoms of the evaporated material can be introduced to the crystal lattice as electrical contacts are created.

Techniques such as Electron Paramagnetic Resonance (EPR) can reveal information regarding the crystal structure surrounding defect atoms. For EPR, a magnetic field is applied to the sample which couples to the magnetic moment of unpaired electrons. The components of angular momentum become quantized, and by applying electromagnetic radiation of suitable wavelengths, transitions between these levels can be induced. Observations of the absorption of the radiation can be correlated to the defect structure or used to determine the chemical identity of defects. A technique known as Nuclear Magnetic Resonance (NMR) is similar to EPR, only the applied field interacts with the magnetic moment of atomic nuclei.

However, one of the most widely used methods is Photoluminescence Spectroscopy (PL). PL involves shining light on a semiconductor material, thereby creating electron-hole pairs, and observing the energy of emitted photons after carrier recombination processes. The technique can reveal information about ground and excited states, and by perturbing the crystal lattice with magnetic fields (Zeeman measurements) or by subjecting it to uniaxial stress, one can obtain data regarding the fine structure of levels. A detailed description of PL spectroscopy is given in the next section.

The type of spectroscopy used is ultimately dependent on the expected or determined properties of the defect(s) under investigation. Some, such as carbon-phosphorus complexes, are

not thought to be optically active and so are not susceptible to PL at all, although other techniques may reveal them. Since EPR is dependent on the defect containing an unpaired electron, it becomes useless for detecting atoms that do not have such an electronic configuration. Therefore, no single spectroscopic technique is sufficient for a complete characterisation of defects in semiconductors. As previously discussed for the case of silicon, the concentration of growth- and processing-induced defects can vary considerably from sample to sample, making a correlation between different researchers, using different spectroscopic methods, on different materials, extremely difficult. There can often be confusion over something as seemingly trivial as the actual chemical identity of defects, particularly as their concentration decreases to 'threshold' values for any given experimental method.

The usual way of determining the identity of certain defects is an extremely time consuming and laborious affair. Many samples of the same starting material would be identically processed, then examined by various spectroscopic techniques, and those spectra analysed. This would provide a base for all future measurements. If one suspected the involvement of a particular element in a specific, or group, of defects, then that would be introduced into the samples in varying degrees of concentration. The annealing temperature, the effect of storage at room temperature, impurities introduced during the growth, storage, handling and annealing processes, as well as the length of time after implantation/diffusion/annealing that the spectroscopic analysis took place, would all need to remain constant or be factored into the experiment. Subsequent examinations would be used to determine if the increase in number of atoms introduced actually affected the intensity of spectroscopic lines. One would therefore also have to consider that there may be processes which might limit the intensity of these lines, and if more than one element were involved in the defect, the concentration of the secondary element might be a limiting factor.

Isotope substitution is often used, where different isotopes of the atoms believed to participate in a particular defect are added to the crystal. The change in atomic mass can alter the energy position of observed lines, allowing the chemical identity of defects to be established. However, since silicon and other semiconductors contain large numbers of processing-induced defects, it is often difficult to determine if slight changes in line position are due to isotope substitution, or differing strain conditions or crystal geometries. As one moves up the Periodic Table, the relative change in mass between isotopes of heavy elements becomes less pronounced. Therefore, it becomes increasingly difficult to be certain that it is a change in isotope that is responsible for slightly different PL line positions.

Perhaps the most elegant way of solving some of these problems is to introduce radioactive isotopes as defects to the semiconductor. Since each isotope decays with a characteristic half-life, observing spectral changes over time allows the experimenter to determine, with considerable certainty, which elements are responsible for specific spectral features. The use of radioactive isotopes can also provide a way to increase the sensitivity of traditional spectroscopic methods. Spectral features related to radioactive atoms will change in intensity with respect to time, even if the concentration of such defects is extremely low. If an integration of line intensities over a relatively large energy region (in the case of PL) is performed, one would not expect the contribution from background noise to change dramatically between measurements. Changes in background intensity over a period of time can be monitored, compared to the half-life decay rate for the radioactive defects, allowing the identification of defects in lower concentrations than could ordinarily be resolved. The first use of implanted radioactive isotopes with PL took place in the mid-1990's and was undertaken by M. O. Henry *et al.*[12], and R. Magerle *et al.*[13].

Note: Throughout much of the literature the term 'chemical identity' is used to refer to the actual identity of impurity atoms in semiconductors. In the case of introducing radioactive isotopes this is, in my opinion, somewhat misleading. Many defects contain a pair or group of atoms, so the use of radioactive ions will only enable the identification of one of the constituents. Therefore the chemical identity of the defect is not actually established, only the nature of one element. For this reason, I shall use the term 'elemental identity' to refer to the constituent whose identity can be inferred from radioactive decay data.

Section 2: Photoluminescence Spectroscopy

2.1 Photoluminescence and Optical Processes

Photoluminescence spectroscopy (PL) is an extremely elegant, and experimentally simple method of obtaining information regarding the optical and electronic properties of semiconductor materials. The popularity of this technique increased dramatically in the mid-1970s with the development of germanium detectors with high signal-to-noise ratios and by the 1980s, Fourier Transform (FT) spectrometers were being used. Today the resolution of spectrometers is no longer a limiting factor in accurate measurements on semiconductors.

Modern FT spectrometers have resolving powers $\left(\frac{\Delta\lambda}{\lambda}\right)$ of the order of 10^6, enabling hyperfine structure of defect levels to be observed during perturbation experiments. For the purposes of my measurements, these high resolutions were not required. The data presented in *Section 4* was obtained using a BOMEM DA8 Fourier Transform Spectrometer fitted with a liquid nitrogen-cooled North Coast germanium detector. Typical resolving powers used were between 5000 – 10000, corresponding to an error in determining the energy of lines to better than ± 0.1 meV. There is a trend within modern spectroscopic literature to quote the energy of observed lines without any mention of possible errors in those determinations. Many researchers clearly believe that the resolution of their spectrometers is sufficient for them to be confident of their results, but it seems unlikely that all published values were obtained at the theoretical maximum resolutions of the equipment used.

For the experiments reported here, a 532 nm Spectra-Physics Millennia II solid-state laser was used to excite carriers. The general requirement for the wavelength of light is that the photon energy be greater than the bandgap energy ($h\nu > E_{BG}$). Since most PL measurements are conducted at low temperatures, to minimise thermal line broadening and prevent bound electrons and holes from being thermally released from defects, the laser power must be sufficiently low to prevent heating of the material. Typical powers used were less than 1 W cm^{-2} unfocused on the silicon, which is adequate for optical excitations. An Oxford Instruments CF1204 cryostat was used to cool samples, generally to temperatures between 3.3 and 10 K, with an error of approximately ±0.1 K.

Temperatures were read and heaters set by an Oxford Instruments ITC-4 controller connected to a Rhodium-Iron sensor located on the sample stick.

Laser light of 532 nm penetrates approximately 1 μm into silicon and is absorbed by carriers. Electrons are excited to the conduction band, leaving corresponding holes in the valence band. These electron-hole pairs relax to energies near the band edges, and can become bound together by their mutual Coulombic attraction. The resultant neutral composite particle is referred to as an *exciton* and can diffuse through the crystal at low temperatures. Typical diffusion lengths are of the order of several hundred microns. As excitons move through the lattice they recombine or become bound to defects. These bound-excitons can be freed by thermal activation or can recombine at the defect itself. There are many recombination processes, details of which are given by Basu[1], but only those that are radiative are of interest here since the emitted photons can be detected.

Band-to-band recombination of electrons and holes is the most obvious process, but since silicon is an indirect bandgap material this requires phonon assistance. The interaction of three particles (an electron, phonon and photon) to achieve this is less probable than other paths at low temperatures. The electron life-time in the excited state is therefore relatively long, and it is more likely to be involved in non-radiative transitions, such as those involved in Auger processes. Correspondingly, the recombination of free-excitons has low probability at these temperatures. The energy of the emitted photon is simply related to the bandgap energy E_{BG} and the internal Coulombic binding energy E_I of the free-exciton:

$$h\nu = E_{BG} - E_I \qquad (1)$$

Recombination of free-excitons does not always require phonon assistance if the silicon has high doping or dislocation concentrations.

However, from the perspective of PL measurements the most important process for the investigation of defects is the recombination of bound-excitons. As with free-excitons the energy of emitted photons is dependant on the bandgap energy and the internal binding energy. It is also dependent on the electronic configuration of the defect and the nature of bonds to its neighbouring atoms.

The photon energy can be written as:

$$h\nu = E_{BG} - E_I - E_L \qquad (2)$$

, where E_L is this 'localisation' energy. Therefore, in terms of energy, the positions of spectroscopic lines as a result of bound-excitons are defect specific and related to the binding of those defects to the lattice. Whether or not phonon assistance is required for the coalescence is dependent on the nature of the defect itself. Many defects can act as traps for a number of excitons simultaneously. Such systems are known as *bound multi-exciton complexes* (*BMECs*). *Fig. 2.1* illustrates a variety of recombination paths in semiconductors.

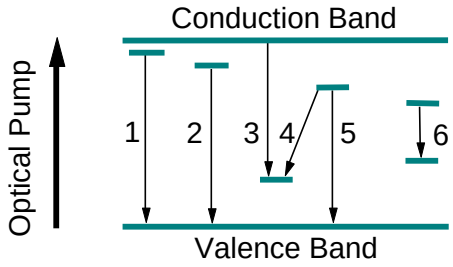

Fig. 2.1: A number of recombination paths for carriers in semiconductors
1 – free exciton (FE); 2 – bound exciton (BE); 3 – electron to acceptor (e,A); 4 – donor to acceptor (D,A); 5 – hole to donor (h,D); 6 – impurity or defect internal transition

One of the major advantages of PL over other spectroscopic techniques, such as DLTS, is that electrical contacts do not need to be applied to the sample. This minimises the possibility that processing will introduce undesirable defects, as described briefly in *Section 1.2*. Samples for PL could theoretically be examined without any form of intervention whatsoever. However, semiconductor materials investigated by PL are usually cleaned of organic contaminants, etched before implantation/diffusion, then annealed afterwards to eliminate damage to the lattice. These processes are described in the next section.

PL is generally not a quantitative technique because many factors can influence the observed intensity of spectroscopic lines. In particular, great care must be taken to ensure that samples are not moved between measurements as the luminescence from different regions of the semiconductor may be the result of entirely different defects. This condition is especially important in dealing with radioactive isotopes, and one must be sure that changes in line intensity are due to

the decay and not the laser simply shining on a different area of the sample. There are also problems involving the storage of semiconductors between measurements. It is possible that thermal dissociation of some defects can occur at room temperature, for example the 'FeB'-related defect described in *Section 4.3*. Considering that it is experimentally difficult (and very expensive) to maintain liquid helium temperatures for extended periods of time, and that the desire is to minimise the duration samples sit at room temperature, isotope half-lives must be short enough that their decay can ideally be followed over the course of a few hours to a few days. Localised laser heating of samples is another factor which can, in terms of the quality of data obtained, negatively influence the intensity of features. Where possible, the angle at which the laser is incident on samples must also remain constant as alterations in the 'skin depth' of penetration may cause different defects to be involved in luminescence.

2.2 Introduction to Vibronic Band Structures and Isotope Substitution

During photoluminescence the laser light causes electrons at optical centres to change orbitals, altering the nature of chemical bonds between the defect and its neighbouring atoms. Therefore one can reasonably assume that if there is a change in the molecular bonding, there will be a corresponding change in the equilibrium position and possibly the vibrational frequency of the defect. The following discussion is based on that given by G. Davies[2].

If we assume a one-dimensional model, and imagine that the defect vibration is simple-harmonic in nature, the vibrational potential of the ground electronic state can be written as:

$$V_G = \tfrac{1}{2}\, m\omega^2 Q^2 \qquad (3)$$

where m is the effective mass of the defect, ω is the vibrational frequency, and Q is the magnitude of the vibrational displacement. In the excited electronic state, the vibrational potential will be:

$$V_E = E + \tfrac{1}{2}\, m\omega^2 Q^2 \qquad (4)$$

where E is the energy of the excited electronic state relative to the ground state. However, since the centre will no longer be stable at the initial position, it relaxes through an energy E_R to a new equilibrium position Q_0. *Equation (4)* becomes:

$$V_E = E + \tfrac{1}{2}\, m\omega^2(Q - Q_0)^2 - E_R \qquad (5)$$

assuming that the effective mass and vibrational frequencies remain the same in both states. In silicon, this is a good approximation. For any given electronic energy state, there is a range of vibrational modes. I will assign the quantum numbers *n* for modes within the ground state, and the number *m* for similar modes in the excited state. At low temperatures the absorbed light will cause excitation of the defect to the higher energy state and to the ground vibrational mode ($m = 0$). During the de-excitation process, the defect can stay in this mode ($n = m$), and the photons produce a spectral line known as the *Zero Phonon Line* (*ZPL*). This is sometimes also referred to as the *No Phonon Line* (*NPL*). Alternatively, the optical centre can change to higher modes ($n > m$), in which case some of the photon energy is lost towards stimulating this higher vibrational mode. These photons will therefore appear at the low-energy side of the ZPL and are known as *Stokes* lines. At higher temperatures, the probability that the excited defect will be in a higher vibrational mode increases. This allows transitions where ($n < m$), thereby inferring that excess phonon energy contributes to the photon. These photons appear as *anti-Stokes* lines on the high-energy side of the ZPL. A diagrammatic representation of these processes is given in *Fig. 2.2*.

One can define a dimensionless parameter, known as the *Huang-Rhys Factor (S)*, as:

$$S = \frac{E_R}{\hbar\omega} \qquad (6)$$

where E_R is the relaxation energy described above. The relaxation energy is dependent on how the electronic energy of the defect is affected by its vibrational changes. Therefore, the value of the Huang-Rhys factor is useful as an indication of the coupling strength between the vibrational and electronic states of a defect.

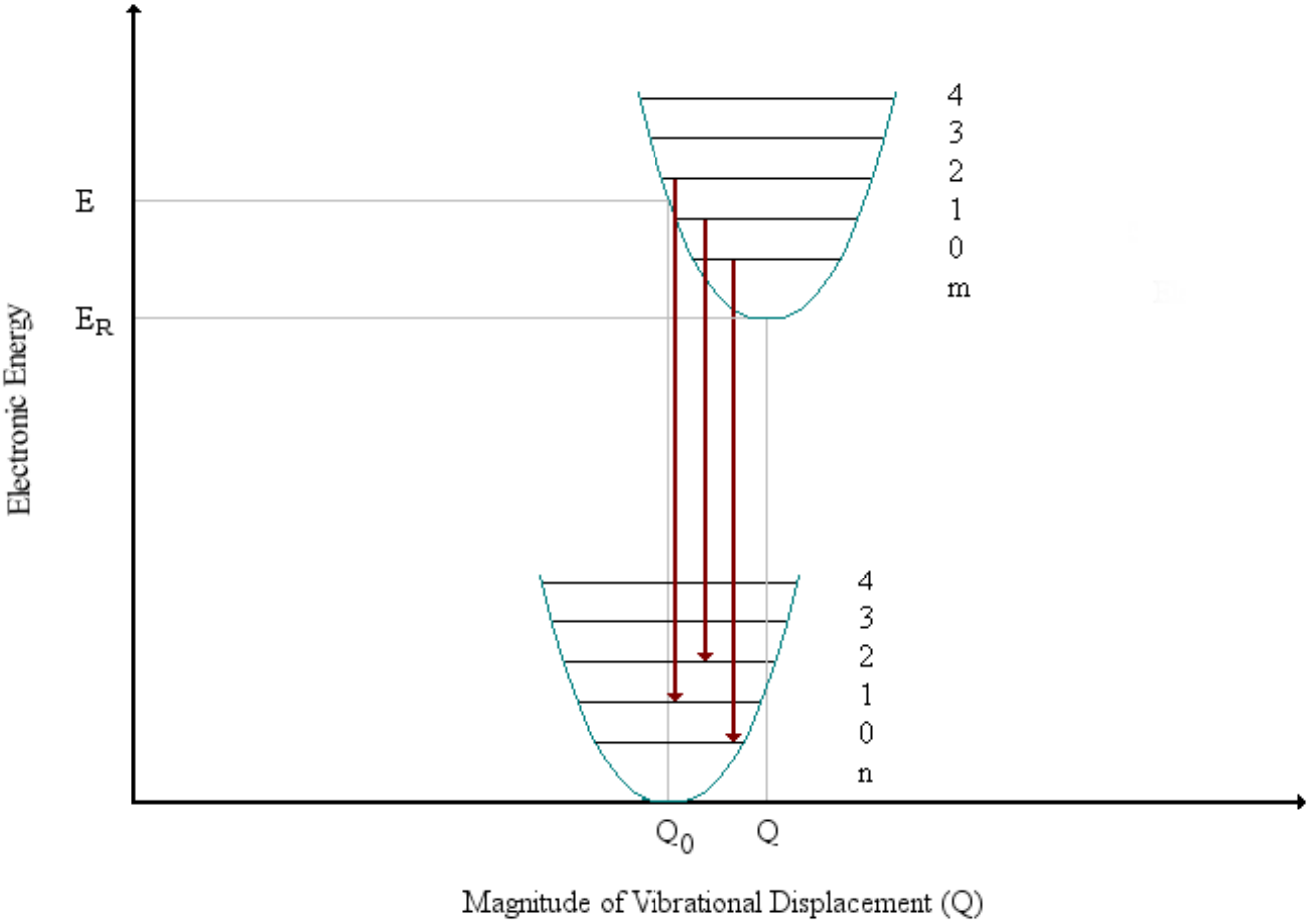

Fig. 2.2: Diagram illustrating the transition of a defect between electronic states and vibrational modes

At low temperatures, transitions primarily from the ground mode ($m = 0$) of the excited state occur to modes where ($n > m$) or ($n = 0$). The relative intensity of PL Stokes lines compared to the ZPL line can be written in terms of the Huang-Rhys factor:

$$\frac{I_{0n}}{I_{ZPL}} = \frac{S^n}{n!} \tag{7}$$

where I_{0n} is the intensity of the line corresponding to a transition from the ($m = 0$) mode in the excited electronic state to the nth mode within the ground state, I_{ZPL} is the intensity of the Zero Phonon Line, and S is the Huang-Rhys factor.

Spectroscopic bands can contain a number of ZPLs, corresponding to transitions from different excited states to ground states for a particular defect. *Fig. 2.3* shows transitions from two excited levels to the same ground level. Providing the vibrational modes remain unchanged, and involve an ($n = m$) transition, both will be observed as a distinct ZPL.

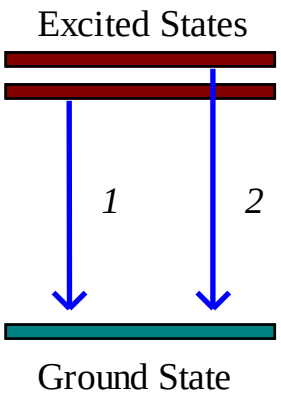

Fig. 2.3: Transitions between two excited states and a common ground state. If the vibrational modes remain unchanged, both will be observed as a ZPL

As one increases the temperature, the probability rises that the higher energy state becomes occupied. The relative intensity of the spectral line corresponding to transition *2*, with respect to *1*, depends on temperature according to:

$$\frac{I_2}{I_1} = A.\exp\left(-\frac{\Delta E}{kT}\right) \tag{8}$$

where ΔE is the energy separation between the excited states, and T is the temperature. The value of A is dependent on the degeneracy of each level g, and the transition probability f:

$$A = \frac{g_2 f_2}{g_1 f_1} \tag{9}$$

From *Equation (8)*, if one were to plot the natural log of the intensity ratio of ZPLs against reciprocal temperature, for a range of temperatures, the slope of the resultant line would give the

energy separation $\frac{\Delta E}{k}$. The intercept of this line with the intensity axis (as $T \longrightarrow \infty$) would give the value of the natural log of *A* from which the value of the product $\frac{g_2 f_2}{g_1 f_1}$ can be deduced. Plots of this sort are used in *Section 4* to determine these parameters for a Hg-related defect.

From *Equation (5)*:

$$V_E = E + \tfrac{1}{2} m\omega^2 (Q - Q_0)^2 - E_R$$

it is clear that the magnitude of the vibrational potential is dependent on the effective mass *m* of the defect. For low mass nuclei, the relative change in mass between isotopes can be quite large. A deuteron (containing a proton and neutron), for example, is 50% more massive than a hydrogen nucleus containing just a single proton. A comparison between two samples diffused with each isotope will reveal a relatively large change in the positions of the ZPL, Stokes and anti-Stokes lines within a hydrogen-related vibronic band[3].

Although isotope substitution is a reliable means of determining the identity of a defect, it still suffers from a number of problems. The most obvious of these is that as one moves up the Periodic Table, the relative difference in the mass between isotopes of heavy elements becomes less pronounced. Since silicon contains high concentrations of processing-induced defects, there may be small changes in the observed energy of spectroscopic lines due to slight differences in the crystal geometry or hydrostatic pressures. For defects with large masses, this makes it difficult to determine if energy positions are related to the change in isotope or some other factor. There is also the potential problem of obtaining sufficient quantities of less abundant isotopes.

Usually crystals of the desired defect material would be heated and the vapour passed through a mass-spectrometer to select the required isotope. These would then be implanted into the semiconductor. Radioactive ion implantation generally involves the use of nuclear fission reactions to produce the desired ions, ensuring that natural limitations regarding the abundance of materials can be overcome. In order for radioactive isotopes to be used successfully for chemical identification of defects, one must establish that the PL intensity is proportional to the concentration of implanted ions. There are a number of good examples within the literature illustrating the procedures necessary to meet such criteria[4,5].

Section 3: Sample Preparation, Implantation, and Annealing

3.1 Sample Preparation

All of the samples used for the following measurements were taken from commercial silicon wafers. Both Float-zone and Czochralski n- and p-type materials were used, with doping concentrations of 5×10^{14} cm^{-3} for FZ silicon and 3 – 5×10^{14} cm^{-3} for CZ material. The doping impurities were boron for p-type and phosphorus for n-type. Further information regarding the nature of the samples will be given during discussions relevant to the Hg- and Au-related defects themselves.

Samples were cleaned and etched using an RCA treatment. Organic contaminants were removed from the samples by washing them in either boiling or room temperature methanol. After rinsing with distilled water, trichloroethylene was subsequently used to remove any remaining methanol from the surface regions of the silicon. A further wash using distilled water was sufficient to dissolve the trichloroethylene. The samples were etched in a 10:1 solution of nitric (HNO_3) to hydrofluoric (HF) acid, respectively. For a solution of 20 ml HNO_3 to 2 ml HF, the etch removes approximately 20 μm of Si in 30 seconds at room temperature. For the purposes of my studies the length of time required for etching was not significant and could be visually determined because the silicon becomes highly reflective when the surface layers are removed. This relatively simple sample preparation is one of the major advantages of PL spectroscopy.

3.2 Introduction to Radioactive Ion Implantation

There are essentially three methods by which defects can be introduced into semiconductor materials. The first is simply to add impurities to the melt during the crystal growth process. The second is to diffuse atoms from the surface region into the lattice. Whilst these are widely applicable, they are not suitable for the introduction of radioactive isotopes due to possible problems in obtaining sufficient quantities of a specific isotope. Since both techniques generally require large amounts of defect material, the safety hazards would be significant if radioactive material was used. The third technique is implantation, whereby ions of the required defect element are accelerated towards the sample surface. Implantation is ideal for introducing radioactive

isotopes, as standard mass-separation techniques can be used to filter out unwanted nuclei. However, implantation does produce significant damage to the crystal lattice which must be removed by annealing.

Since we wished to investigate the effects of certain Hg- and Au-related defects on silicon, it was necessary to pick suitable radioactive isotopes. The half-life decay time $T_{1/2}$ of radioactive nuclei is related to the activity $\frac{dN}{dt}$ by the expression:

$$\frac{dN}{dt} = -\frac{\ln 2}{T_{1/2}} N \qquad (10)$$

where N is the number of radioactive nuclei in the sample. The SI unit for activity is the becquerel (Bq), which corresponds to one decay per second. Another commonly used unit is the curie (Ci), where 1 Ci = 3.70×10^{10} Bq.

In order to minimise radiation exposure, which is dependent on the activity, one requires an isotope with a relatively long half-life. This also, in theory, ensures that there is a sufficient concentration of defects for examination after samples have been transported from the implantation facilities to spectroscopic equipment. The primary decay line used was ${}^{197}_{80}Hg \xrightarrow{64.1h} {}^{197}_{79}Au$ (stable), with a half-life of 64.1 hours. The number of implanted ions was typically 8×10^{12} per sample. Using *Equation (10)*, the activity of a single sample is approximately 2.4×10^{6} Bq or 65 mCi. Since eight samples were placed within the implantation chamber, the total activity after implantation was about 0.5 Ci.

3.2.1 Overview of ISOLDE Operation

This section shall give a brief overview of the Isotope Separator On-Line (ISOLDE) facility at CERN, which was used to implant radioactive ions into silicon, as well as the possible impurities unintentionally introduced into samples during Hg implantation. The purpose of ISOLDE is to produce a variety of radioactive isotopes, and to allow researchers to separate out and direct specific masses to their respective experiments. This ability has ensured the use of the facility in many research fields, including nuclear and atomic physics, solid-state physics, medical science and material science. *Fig. 3.1* is an overview of the ISOLDE General Purpose Separator (GPS)[3], and a more detailed description of the equipment is given below.

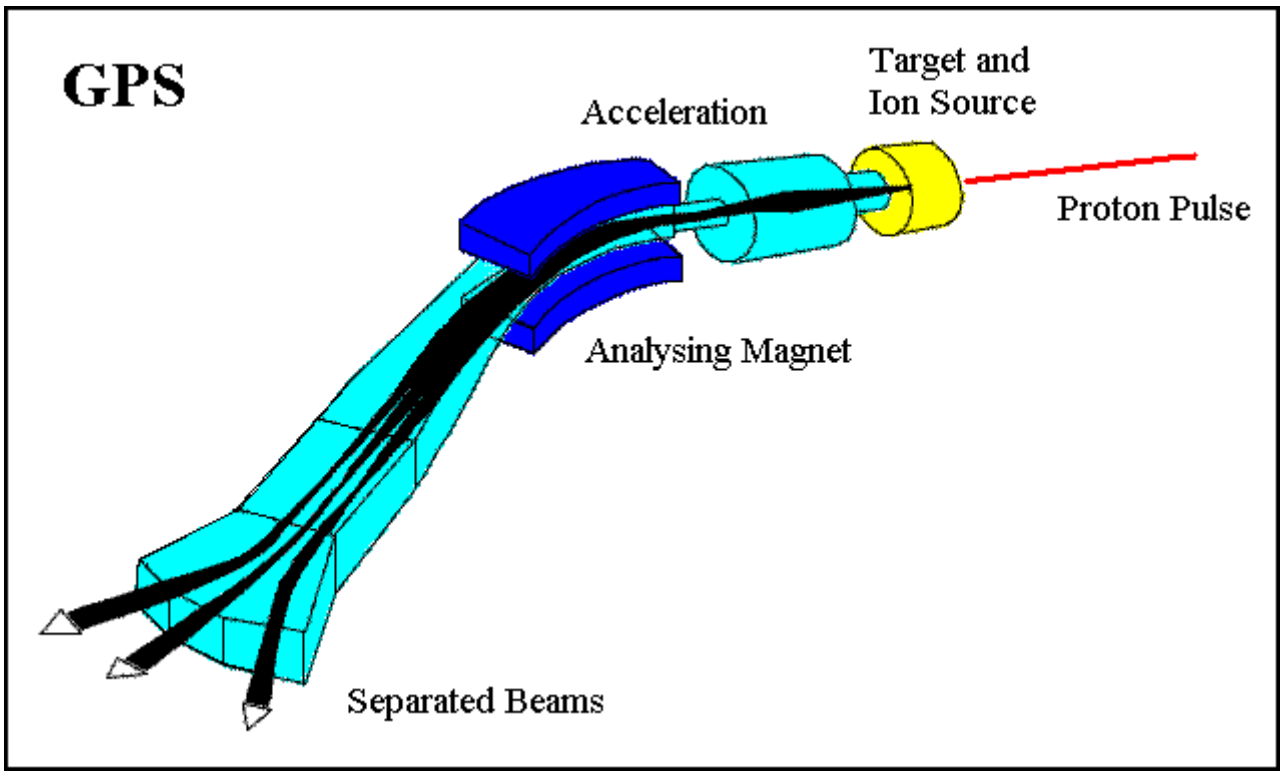

Fig. 3.1: Overview of the General Purpose Separator at ISOLDE. A target is bombarded by 1 GeV protons, causing a range of fragmentation reactions in the target nuclei. The product atoms diffuse through the target material and are accelerated towards an analysing magnet. This separates the radioactive isotopes horizontally by mass, allowing three different isotopes to be guided to the respective experiments

The PS Booster

The Proton Synchrotron Booster (PSB) is the first step in the process of producing radioactive isotopes. Protons are passed from a Linac to the PSB, which consists of four synchrotrons stacked vertically. The Booster accelerates these protons to energies of 1 GeV. About half are diverted to the much larger Proton Synchrotron (PS), which in turn supplies particles to CERN's high-energy machines and colliders. The rest are theoretically available for the ISOLDE equipment.

The PSB emission is not continuous, with twelve pulses in each supercycle of the synchrotrons. Each pulse lasts approximately 2.4 μs and ISOLDE typically receives about six pulses per supercycle (pps). Based on the implantations I performed at the facility, each pulse contains 7×10^{12} protons although some sources indicate that the intensity can be pushed to 3.2×10^{13} protons per pulse (ppp)[1].

ISOLDE Targets

Protons are delivered from the PSB to impact on the two ISOLDE targets via an underground transfer line. Great care was taken in the design and development of the target area due to the large amount of radiation that is produced by the resultant nuclear fragmentation reactions. The entire structure is buried under 8 m of earth and shielded with concrete and steel blocks. Special filtration systems store contaminated air in steel tanks, and ensure an interior pressure slightly below that of the atmospheric pressure outside the facility. This minimises the amount of radioactivity emitted into the surrounding environment. Targets are handled by two state-of-the-art robotic arms in order to minimise the radiation exposure of personnel, and are stored in-house after use until their activity decreases to more manageable levels.

ISOLDE features two mass separators - the General-Purpose Separator (GPS) and the High Resolution Separator (HRS). These can be operated together in a time-sharing mode, hence the requirement for two target zones. Whilst one target is situated directly in line with the proton beam, the second requires the beam to be diverted through a bend of 400 mrad using magnets. Since the PSB output is pulsed, the bending magnets can be synchronised to alternately switch which of the targets is bombarded by the protons. Both the GPS and HRS can therefore use the same target

areas, loading mechanisms and proton transfer line, and can be operated simultaneously due to this elegant engineering design.

Targets of carbides, metal/graphite mixtures, foils of refractory metals, molten metals and oxides can all be used at the ISOLDE facility. The choice of target material obviously depends on the isotopes required for experiments. In total, more than 60 elements are available as on-line produced ion beams[2]. Experiments requiring certain isotopes are therefore scheduled to coincide with the appropriate target material.

For the purposes of producing Hg (and other elements such as Au and Pt), a Pb target is used. When energetic protons strike the Pb atoms, they produce a range of elements and corresponding isotopes through complex spallation, fragmentation and fission reactions. The yields, available isotopes and target materials can be found on the ISOLDE webpage[3], or in technical manuals published by CERN[4]. The target must remain molten, as the high temperature ensures that the produced elements will diffuse through the material and be released from it. Allowing protons to impact on a solid target would result in it retaining radioactive isotopes, and the safety hazards associated with its activity would be substantially increased.

A current of some 500 A is passed through the Pb to heat it to a temperature of around 500 – 550 ˚C. Once the proton beam is incident, however, the nuclear reactions cause considerable heating of the target and the current must be reduced to around 120 A, depending on the intensity and number of pulses of protons. A molten metal target is characterised by a long release time of isotopes, typically with a time constant of the order of 30 seconds. Since the proton pulse duration and supercycle repetition rate are very much shorter than this, the use of molten metal targets results in a continuous stream of isotopes.

As Hg and other reaction products are emitted they can cool and attract free electrons. The ultimate purpose of creating these atoms is to separate out specific isotopes with magnets, so it is necessary to ensure the ionisation of the atoms released. In the case of the Pb target, the liberated atoms are passed through a Xe plasma-heated transfer line. From here they are guided down a beam-line using accelerating voltages and steering quadrupoles and diverted into the GPS separator.

The isotopes released from the target are often referred to as the ‘radioactive beam’, and whilst I shall use this convention throughout the following discussion, it should be noted that many stable isotopes are also produced in the nuclear processes.

The General Purpose Separator (GPS)

The GPS is designed to allow three different isotope beams, within a certain mass range, to be delivered simultaneously into the experimental hall. Mass separation is achieved through the use of a 0.45 T-maximum electromagnet with a bending angle of 70˚ and a 60 kV acceleration gap at its front end. This effectively means that the average energy of implanted ions is 60 keV. The High Resolution Separator (HRS), which shall not be discussed here, features two magnets - the first with a bending angle of 90˚ and the second with 60˚. As the radioactive beam passes through the GPS magnet it is separated by mass horizontally across the output. The current to the magnet is calculated so that a specific isotopic mass is deflected around the bend radius and is central at the magnet output. This is referred to as the ‘centre mass’ beam. The isotope beams deflected each side have correspondingly greater or lesser masses.

From here the separated beams are guided into the so-called ‘switchyard’, which consists of pairs of cylinder-shaped electrostatic deflectors. These can be moved horizontally across the magnet output, enabling researchers to choose and deflect a high and/or low mass isotope (relative to the centre mass) to separate lines. Provided these high and low mass beams are within ±15% of the centre mass, the GPS can operate with three isotopes simultaneously. For the implantations I performed with ^{197}Hg, the high mass beam-line was used since these atoms were more massive than Hg isotopes required by other ISOLDE users.

The Sample Chamber

From the switchyard, the radioactive beams are accelerated through the appropriate transfer lines, guided by sets of steering quadrupoles. At the end of each is a metal gate that prevents the ions from impacting on the samples. The number of atoms implanted is simply controlled by the length of time the gate remains open.

Up to eight samples can be mounted on a precision-drilled aluminium holder, and each is held by a small clamp. When placed in the end chamber a stepper-motor moves the holder laterally, bringing each sample in turn to the centre position. Directly in front of the holder, between it and the beam-gate, is a small collimator and for the implantations I performed, a square collimator 5 mm×5 mm was used.

To reduce the implantation damage and to ensure an even distribution of isotopes across the sample material, the radioactive beam was swept vertically and horizontally across the collimator using alternating voltages on deflector plates. The collimator therefore acts as a screen, limiting the size of the implantation area. The number of atoms at the collimator can be determined by measuring the current through it. In order to determine the length of time the beam-gate should remain open, and hence the number of atoms implanted, it is also necessary to measure the current of the radioactive beam at the sample holder.

Computer software in the ISOLDE control room integrates these currents and determines the number of ions implanted. However, since these implanted atoms may be decaying with the emission of β^- and/or α-particles, these charges may contribute slightly to the current measured. One can determine this 'dark current' by closing the beam-gate after the calculated time has elapsed. The current measured on the sample holder is then the current related to the activity of the sample rather than the ion beam, and adjustments in the exposure time can be factored in. A diagram of the ISOLDE equipment is shown in *Fig. 3.2*.

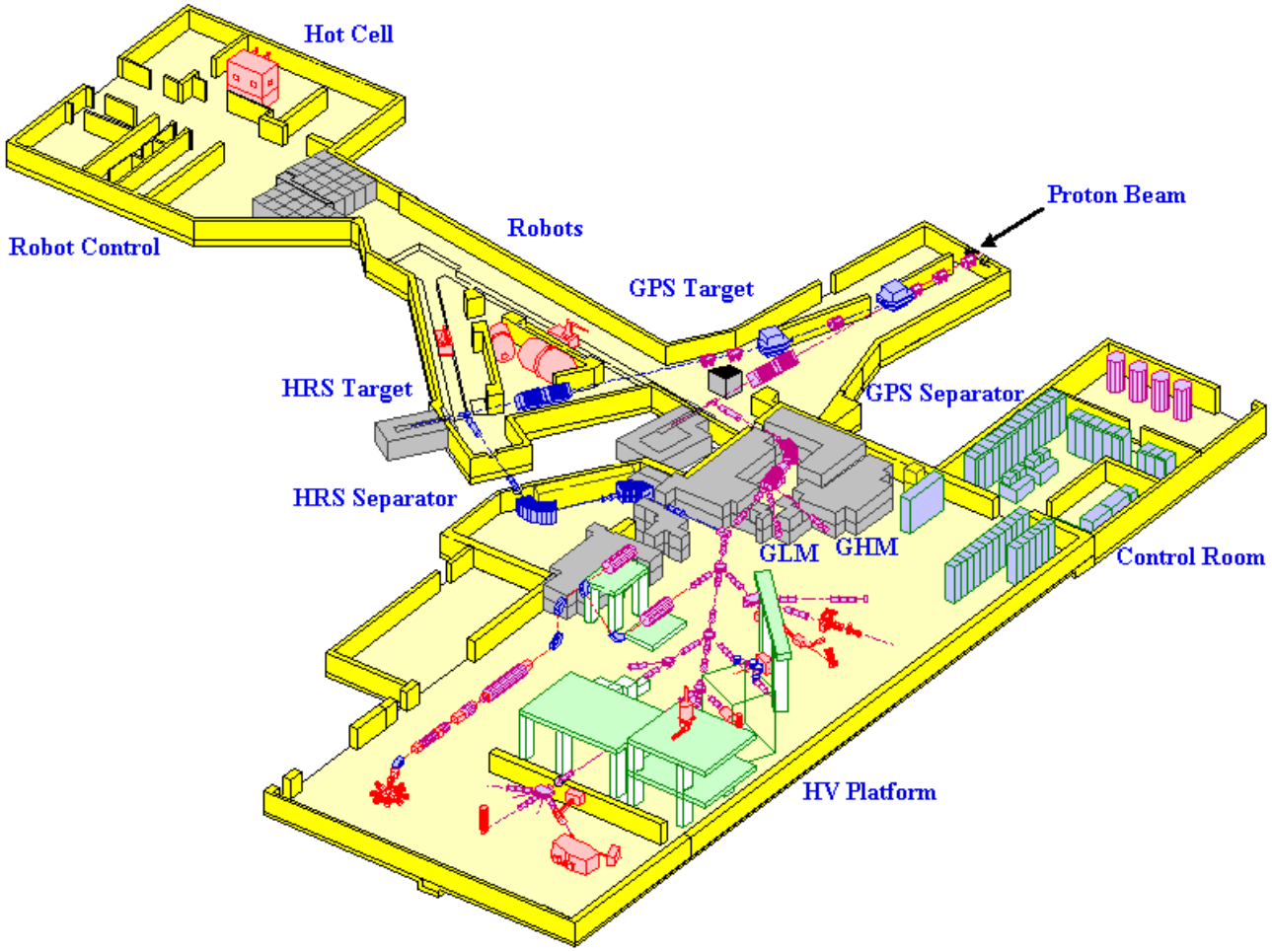

Fig. 3.2: Illustration of the ISOLDE facility, taken from the CERN website[3]. The proton beam impacts on the GPS target, and the reaction products are guided through the GPS magnet (separator). For the implantation of ^{197}Hg the high-mass (GHM) line was used. The centre-mass beam can be transferred to many experiments simultaneously. The GLM line is used for the low-mass isotopes. This effectively means experimenters can work with one of three isotopes simultaneously. ISOLDE's design is largely revolutionary and forms the basis of similar facilities at such institutions as FermiLab

3.2.2 Ion Yields and Impurities

Fig. 3.3 shows the yield of Hg isotopes from the molten Pb target, with 6 pps and 7×10^{12} ppp. This graph is for a previous incarnation of the ISOLDE equipment, and the newer facility has either equivalent or slightly better yields. It was compiled from data taken from the ISOLDE User's Database, available on the Web from the address referenced previously[3].

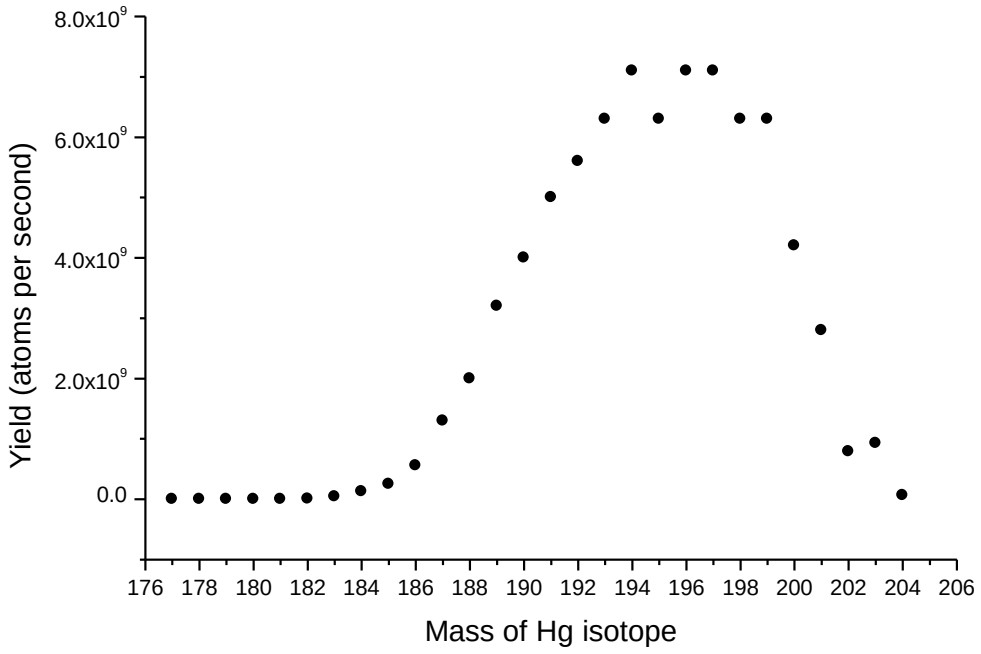

Fig. 3.3: Plot of ISOLDE (Pb) target yields for isotopes of Hg. These figures were experimentally determined by ISOLDE technicians

For the majority of my experiments a dose of 2×10^{12} atoms cm^{-2} of ^{197}Hg was required, but since a 5mm×5mm collimator was used, the total number of atoms implanted was simply four times the dose or 8×10^{12} atoms. The yield from the Pb target, as illustrated in the previous figure, is approximately 7×10^{9} atoms per second giving a theoretical implantation time of about 19 minutes per sample. If one assumes that the beam-sweep will be activated and 50% of separated atoms are incident on the collimator as a result, one can expect to double this time. This rough calculation gives an idea of the time necessary for implantations, although there can be dramatic variations depending on the numbers of protons available and the temperature of the target. Some of the samples I implanted took 20 minutes or less with 10 pps.

It is important to note that the mass separation procedure at ISOLDE does not guarantee a pure isotopic beam. During the bombardment of the Pb target with protons, a wide range of elements and associated isotopes are produced. It is very possible that elements besides Hg with an isotopic mass of 197 are also created, and that these are constituents of the 'radioactive' beam. Fortunately the majority of produced isotopes *are* radioactive, so one can determine the identity of most atoms implanted and their relative concentration using γ-ray spectroscopy. Of particular concern to me was the possibility that ^{197}Tl or ^{197}Pt was produced in the target reactions.

Atomic nuclei of elements with similar mass have similar nuclear configurations. This means that, during radioactive decay processes, one would expect there to be a similarity in the energy of γ-rays emitted. In order to determine the elemental identity of isotopes implanted into silicon, it is necessary to find γ energies that are unique to that particular element or demonstrate that the ratio of intensities of spectral lines matches established data. The table below shows the energy and relative intensity of γ-ray lines from ^{197}Hg, ^{197}Tl, and ^{197}Pt and is taken from data available at the ISOLDE Users' Office.

^{197}Hg		**^{197}Tl**		**^{197}Pt**	
γ energy (keV)	Relative intensity	γ energy (keV)	Relative intensity	γ energy (keV)	Relative intensity
				53.10	1.07%
77.35	18.0%			77.35	17.1%
130.2	0.22%			130	0.11%
133.98	34.4%	133.99	2.0%		
		152.22	7.2%		
164.97	0.27%				
191.364	0.61%			191.437	3.7%
201.8	0.07%			202	0.03%
268.71	0.04%			268.78	0.23%
279.0	5.0%			279	2.4%
		308.6	2.2%		
				346.5	11.1%
409.1	0.01%			409	>0.01%
		425.84	12.9%		
		433.14	2.5%		
		577.97	4.4%		
		674.28	1.46%		
		792.06	1.8%		
		857.18	2.1%		
		1411.34	4.5%		

Samples of ^{197}Hg were placed together in plastic containers and examined collectively with a γ-spectrometer. Both ^{197}Hg and ^{197}Pt have γ lines at 77.4 and 191.4 keV. However, for Hg the intensity ratio is 18% : 0.6% (30 : 1), whereas for Pt the corresponding ratio is 17% : 3.7% (4.5 : 1). From the γ-spectrometer used, the observed intensity of the 77.4 keV compared to the 191.4 keV line was 5×10^5 : 1.6×10^4 counts, or 31:1. This ratio not only indicates the presence of ^{197}Hg, but shows that ^{197}Pt does not contribute significantly to the spectrum and is not introduced in appreciable quantities to the samples. The Pt-specific line at 346.5 keV was not discernable from background noise. It should be noted that although these measurements indicate the absence of Pt for samples containing ^{197}Hg, it cannot rule out the possibility that Si implanted with other isotopes will reveal Pt defects. As will be discussed in *Section 4*, spectroscopic analysis of some samples does indicate the presence of Pt impurity centres.

The 133.98 keV line has a relative intensity of 34% for ^{197}Hg. One would therefore expect it to appear approximately twice as intense as the 18% (5×10^5 counts) 77.4 keV line discussed above. The measured intensity was 1×10^6 counts as expected.

A fairly weak line at 425.8 keV was also observed, and since this is unique to ^{197}Tl, one can conclude that the samples contain a small amount of thallium contamination. The measured intensity of this 12% line was 3460 counts. Since the 34% (1×10^6 counts) 133.98 keV ^{197}Hg line should only appear approximately three times as intense as this 12% 425.8 keV ^{197}Tl line if equal amounts of Hg and Tl were implanted, the Tl line should have an intensity of about 3×10^5 counts. That the intensity is approximately a hundred times lower than this value indicates that the ratio of implanted Hg:Tl atoms is about 100:1.

3.3 Annealing

The implantation of large mass isotopes at energies of 60 keV can cause considerable damage to the silicon lattice. This must be removed before PL measurements can be made, otherwise defect-related features would become obscured by luminescence related to carrier recombination at crystal flaws. Due to the high acceleration and energies involved, implanted atoms do not necessarily occupy sites they ordinarily would under conditions of thermodynamic equilibrium. This implies that such defects can exhibit entirely different PL characteristics to those of diffused atoms of the same element. Annealing not only removes crystal damage, but causes implanted ions to diffuse through the crystal until equilibrium positions are reached. There are two ways to end the annealing process. The first is to *quench* the sample by dropping it (in a sealed ampoule) into a cold liquid. Quenching freezes the equilibrium conditions present at the annealing temperature because there is little time for the formation of precipitates. The disadvantage is that the rapid temperature change places the sample under stress. The second technique is to allow the semiconductor material to cool slowly. Although this minimises the possibility of damage due to rapid thermal change, it favours the formation of complexes when defects capture additional atoms during the slow cooling process.

The mean projected range of 60 keV Hg ions is of the order of 400 Å, with a straggling of around 100 Å[5]. These figures give a rough impression of the depth distribution of ions and the possible extent of damage as a result of the implantation. We have found an anneal at 1050 °C for 10 minutes, followed by quenching in room-temperature water, is sufficient to remove damage to the lattice and, although a large quantity of Hg diffuses to the surface of the samples, a sufficient number of atoms remain for PL measurements. Ming Wang *et al.* have shown that after an anneal at 700 °C for 30 minutes, the Hg shifts towards the surface of Si, and up to 1000 °C the amount of Hg retained decreases significantly[6]. This fits in with the behaviour as observed, and also suggests that Hg–related defects lie near the surface of Si.

After implantation, samples were sealed in quartz ampoules filled with He to half atmospheric pressure. The inert gas maintains the purity of samples during transport and annealing, and samples were generally not removed from ampoules until after the annealing step. However, for the investigation of the 1004 meV Au-Li defect, discussed in the next section, it was necessary to diffuse Li into the Si. This was achieved by placing a small amount of the Li metal into the ampoule before annealing.

We have found there to be no need to re-etch samples after implantation, and the quality of spectra obtained does not appear to suffer as a consequence. Re-etching samples implanted with Hg may only serve to destroy the defects which lie near surface layers.

Section 4: Photoluminescence Results

4.1 Introduction

Generally, it is necessary to 'normalise' PL spectra relative to some known spectroscopic line. This ensures that variations in experimental conditions, as described in *Section 2.1*, can be factored into the measurements, that meaningful results are obtained, and that comparisons of line intensities can be made between samples. The observed peaks were normalised either to the boron-related bound-exciton line that appears at 8813.3 cm^{-1} (1092.7 meV), or to the TO free-exciton (FE) line at 8849.8 cm^{-1} (1097.4 meV). The intensity of both these lines is very sensitive to temperature, so this type of normalisation procedure was only used to compare different samples at similar temperatures. In the case of observing the same feature in an individual sample over a range of temperatures, the normalisation described above can introduce errors because the bound or free-exciton lines change intensity at a different rate to the defect of interest. This problem is solved by rigorously maintaining the experimental set-up over a number of hours and ensuring that only the temperature is altered before each spectrum is obtained. Although there can be variations due to changes in the temperature of the germanium detector (as well as the occasional spurious data point caused by cosmic γ-ray spikes), these fluctuations are extremely minor in comparison to the effects of even slight changes in laser power or sample position.

Due to the high energy of implantations and the large mass of ions used, annealing of samples is not always sufficient to remove damage-related luminescence. This means that some of the relevant spectral lines can appear on broad features which can give a false impression of the relative intensity of peaks. The effect of such damage-related bands can be removed by plotting a baseline through the data points, then mathematically subtracting this baseline across the entire spectrum.

There are two methods by which to obtain the intensity of a given spectral peak. The first is simply to take the intensity maximum of the line after normalisation, if performed, and baseline removal. The second is to integrate across the entire feature, which determines the total area under the peak. In this case, baseline removal is essential. Integrated intensity not only takes into account the height of lines but also their width, which can be valuable in comparisons of Stokes and anti-Stokes features, or of changes in spectra with respect to temperature.

4.2 Hg-Related Defect

4.2.1 Determination of Relevant Spectral Features

Figs. 4.2.1 and *4.2.2* show regions of the PL spectrum obtained at a sample temperature of 4.4 K for p-type FZ silicon implanted with 2×10^{12} atoms cm^{-2} of stable ^{200}Hg. This implantation was performed at the Instituto Technológico E Nuclear (ITEN) in Portugal, and shall be compared below to samples created at the ISOLDE facility. An identification of lines in regions labelled *1* to *6* can be found in *Table 4.2.1*. The extremely intense broad band structure between approximately 6000 and 6400 cm^{-1} *(1)* has only been reported previously by Henry *et al.*[1].

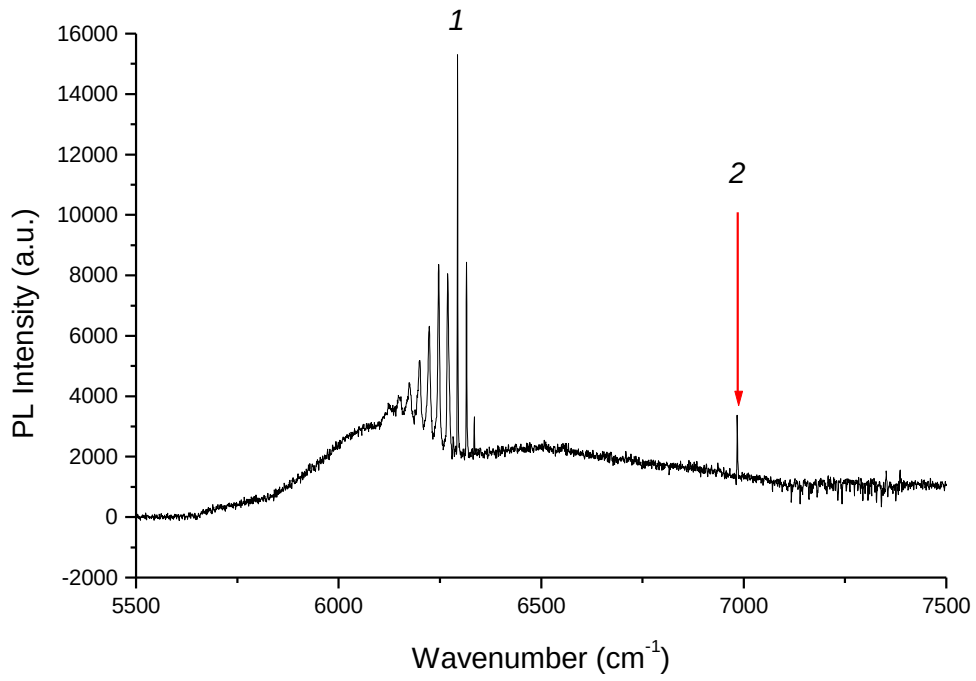

Fig. 4.2.1: Region of PL spectrum at 4.4 K for p-type Si implanted with ^{200}Hg at ITEN, Portugal. The broad band labelled (1) is a feature previously only reported by this group

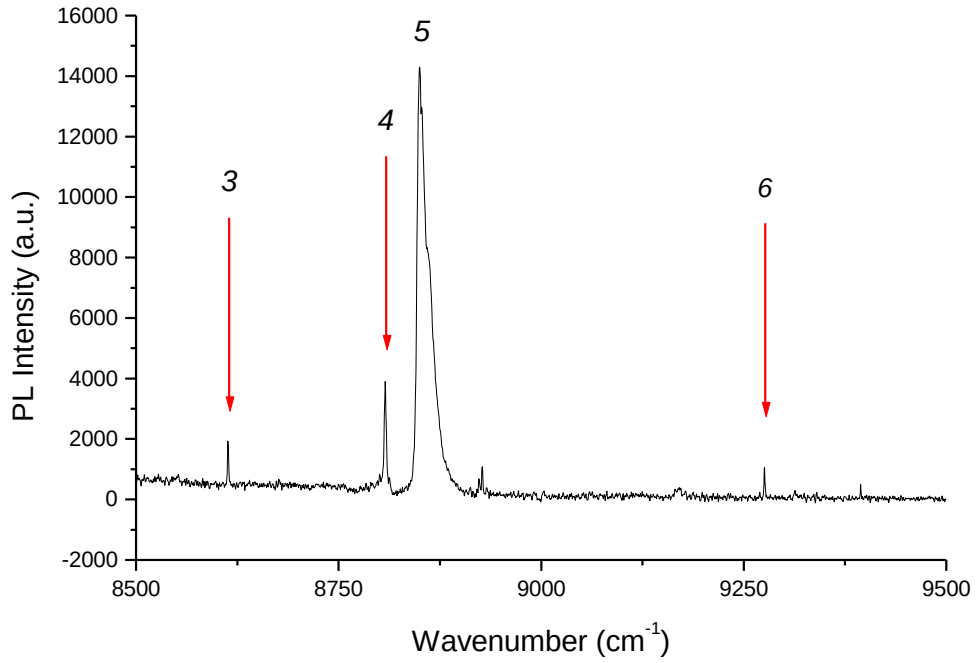

Fig. 4.2.2: Region of PL spectrum for the same ITEN sample as discussed above

Table 4.2.1:

Designation	**Wavenumber (cm^{-1})**	**Identification**
1	-	*Hg-related defect to be discussed in this section*
2	*6984*	*Unknown feature*
3	*8613.4*	*'FeB' defect, discussed in Section 4.3*
4	*8807.5*	*B-related bound-exciton line*
5	*8849.8*	*TO free-exciton line*
6	*9275.3*	*P-related bound-exciton ZPL*

An enlargement of the observed broad feature, for this ITEN sample, is shown in *Fig. 4.2.3*. These lines are believed to be Hg-related, but since the chemical identity of the defect is not relevant to the following analysis, reasons for this assignment are given in a later section. *Fig. 4.2.4* is the same spectral region for a p-type FZ Si sample implanted at ISOLDE. The isotope used was also stable ^{200}Hg, and the dosage was 2×10^{12} atoms cm^{-2}. *Fig. 4.2.5* is an overlay of the spectrum from each sample, illustrating that the general band shape of this feature is similar in both cases.

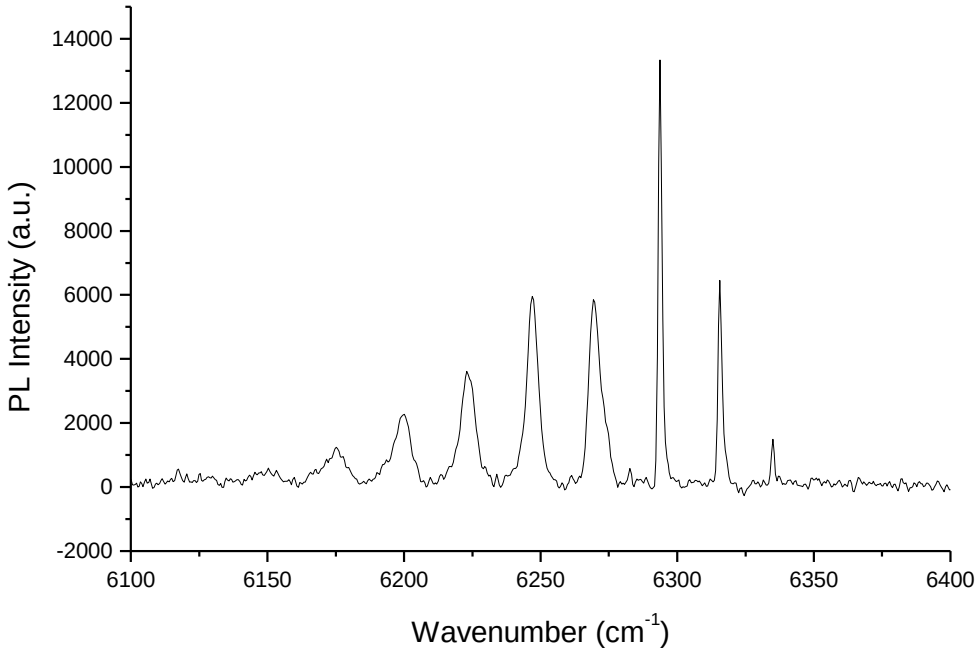

Fig. 4.2.3: Enlargement of the broad feature, at 4.4 K, for a ^{200}Hg-implanted sample from ITEN

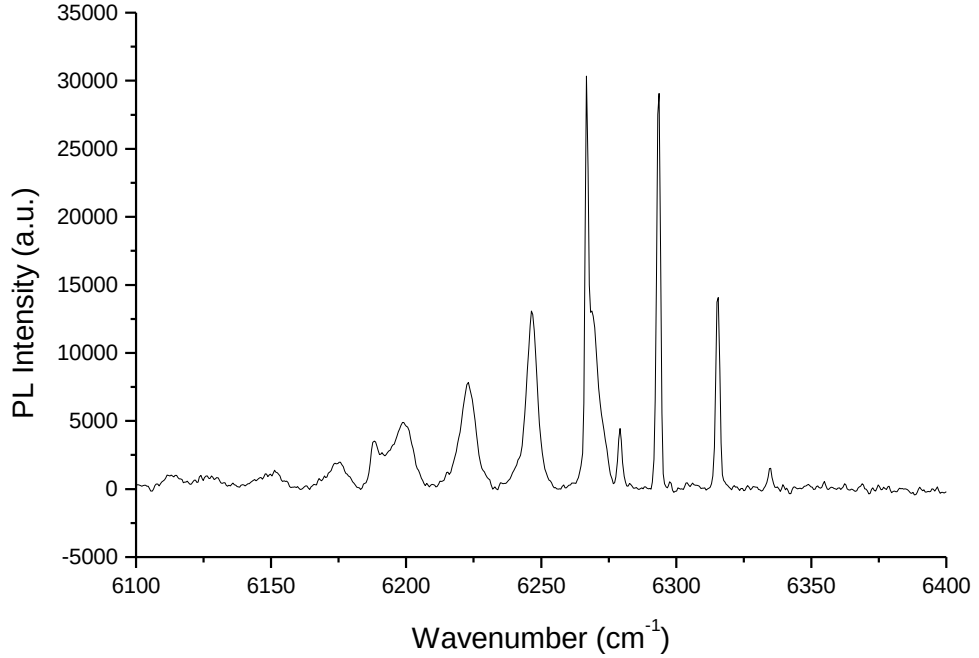

Fig. 4.2.4: Enlargement of the same feature, at 4.4 K, for an ISOLDE sample implanted with ^{200}Hg

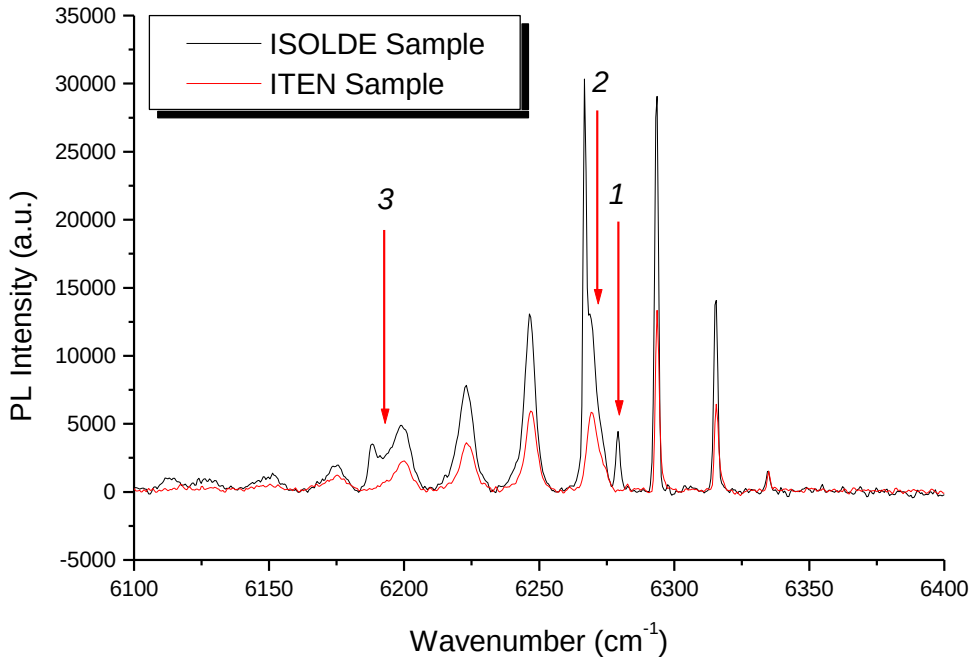

Fig. 4.2.5: Comparison of the spectra for the ITEN and ISOLDE samples. Many of the lines are common to both, but there are a number of unique features found in the ISOLDE-implanted material. These are indicated by the arrows, and are believed to be due to Pt contamination

However, the spectrum from the ISOLDE sample contains a number of features that are not found in the ITEN sample. These include the presence of a new line (*1*), a slight energy 'shoulder' on one of the main peaks (*2*), and a distorted line shape at (*3*). The peak labelled (*1*) has a maximum at 6279.2 cm^{-1} (778.6 meV), and is due to Pt contamination. Henry *et al.* have previously demonstrated that the observed 777 meV Pt-related line[2,3] is made up of two ZPLs – the first occurring at an energy of 777.6 meV and the second at 778.9 meV[4]. It is this second ZPL that corresponds to the line labelled *(1)* seen in the ISOLDE sample. The presence of the Pt-related ZPL at 777.6 meV would explain the slight 'shoulder' labelled *(2)*. The double peak structure at the line *(3)* is due to a phonon replica of this Pt defect. *Fig. 4.2.6* is a comparison between the ISOLDE spectrum and this Pt-related defect, illustrating the above assessment. It should be noted that both spectra were obtained using different spectroscopic equipment, so there may be slight variations in the determined energy position of lines. Nevertheless, the correlation is good and there can be no doubt that the anomalies observed in the ISOLDE sample are due to Pt contamination.

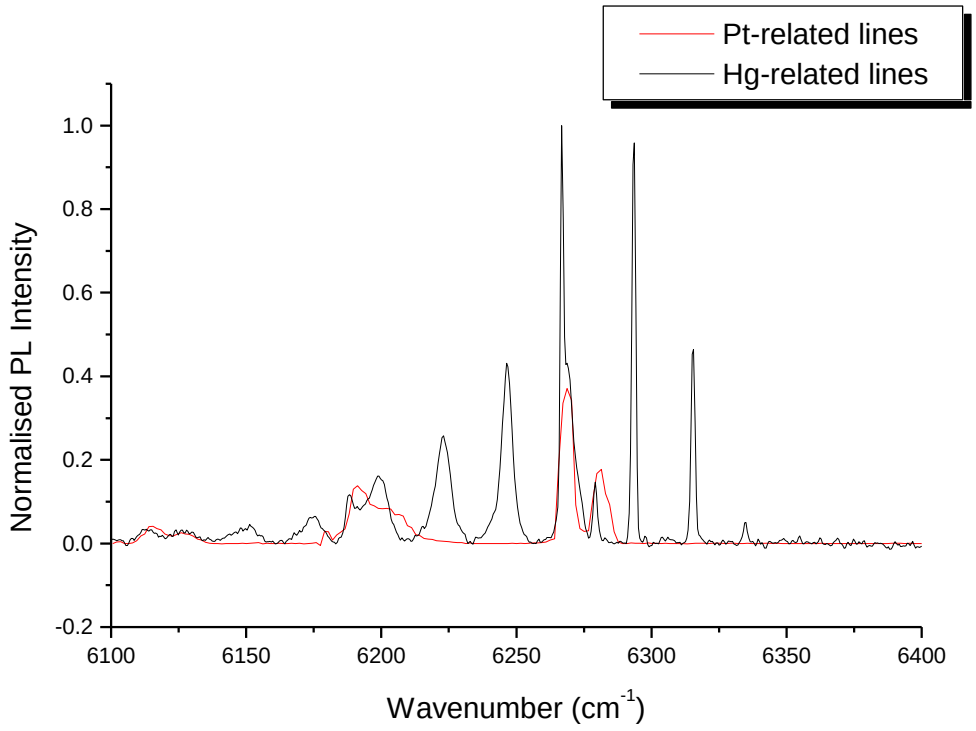

Fig. 4.2.6: Comparison of the ISOLDE spectrum and a previously obtained Pt-related defect[4], illustrating those features that are the result of ^{200}Pt contamination

4.2.2 Analysis of Phonon Sideband

Having established those features that are common to both ITEN and ISOLDE-implanted Si, *Fig. 4.2.7* shows the labelling assignment for each PL line.

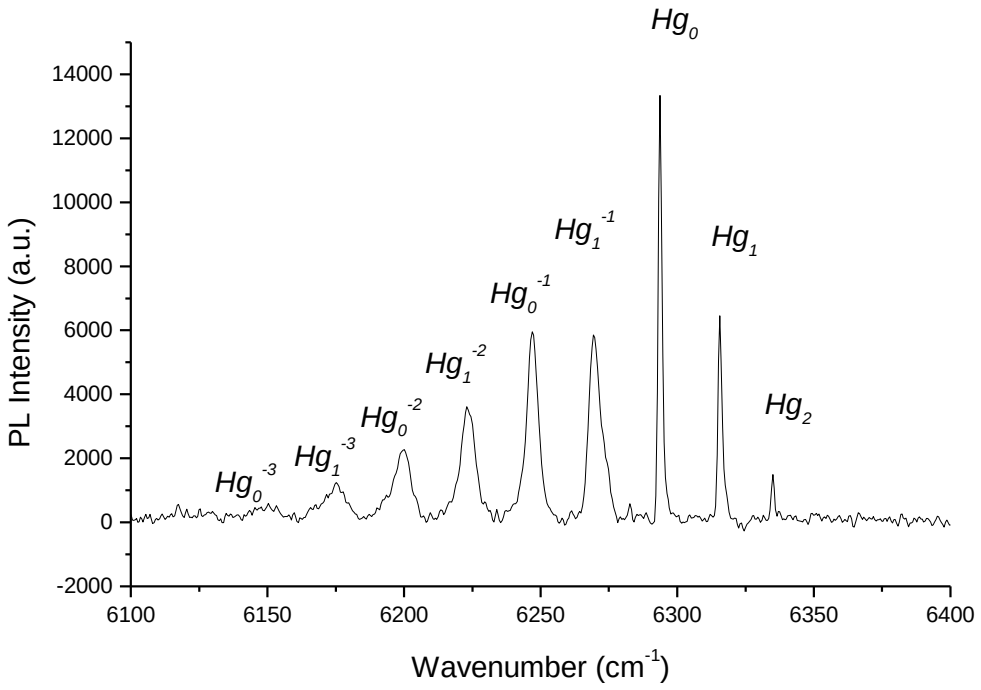

Fig. 4.2.7: The label assignment for those peaks common to both ISOLDE and ITEN samples. This spectrum was obtained at 4.4 K for the ITEN sample

Based on the narrow width of the peak labelled Hg_0, this is determined to be a Zero Phonon Line (ZPL), corresponding to an ($m = n$) transition as described in *Section 2.2*. It has peak energy at 6293.7 cm^{-1} (780.4 meV). The features Hg_1 and Hg_2 are also suspected to be ZPLs, mainly because of their narrow line widths. One would not expect to observe prominent anti-Stokes features at such low temperatures, so that possible assignment of the two higher energy lines can be ruled out. The features labelled Hg_i^{-1} to Hg_i^{-3} are Stokes lines sidebands of the ZPL doublet of Hg_0 and Hg_1, hence the subscript notation in the labelling of peaks. *Table 4.2.2* shows the energy position of the major peaks within the band. There is spectral evidence of more Stokes phenomena, but due to the low intensity, large widths and resultant difficulty in determining peak energy positions, they have not been considered.

Table 4.2.2:

Line Designation	Peak Energy Position (meV)	Phonon Energy (meV)
Hg_2	785.5	**0**
Hg_1	783.1	**0**
Hg_0	780.4	**0**
Hg_1^{-1}	777.4	**5.7**
Hg_0^{-1}	774.6	**5.8**
Hg_1^{-2}	771.8	**11.3**
Hg_0^{-2}	768.9	**11.3**
Hg_1^{-3}	765.6	**17.5**
Hg_0^{-3}	762.6	**17.8**

Based on this data, the vibrational energy separation is approximately 5.7 meV. One can determine the value of the Huang-Rhys factor, as discussed in *Section 2.2*, using *Equation (7)*:

$$\frac{I_{0n}}{I_{ZPL}} = \frac{S^n}{n!}$$

where I_{0n} is the intensity of the line corresponding to a transition from the ($m = 0$) mode in the excited electronic state to the nth mode within the ground state, I_{ZPL} is the intensity of the Zero Phonon Line and S is the Huang-Rhys factor. The values of S are simply given by the ratio between the intensity of the first Stokes lines ($n = 1$) and each of the ZPLs. *Table 4.2.3* shows the integrated intensity of these lines at 4.4 K, and the values of the Huang-Rhys factors based on this ratio.

Table 4.2.3:

Line Designation	Value of n	Integrated Intensity of Peak (a.u.)	Value of Huang-Rhys factor (S)
Hg_0	0	25126	-
Hg_0^{-1}	1	33937	**1.4**
Hg_1	0	13886	-
Hg_1^{-1}	1	35748	**2.6**

The value of the relaxation energy E_R can be calculated from S using *Equation (6)* (*Section 2.2*):

$$S = \frac{E_R}{\hbar\omega}$$

where $\hbar\omega$ is the phonon energy. From *Table 4.2.2*, based on spectroscopic observation, the separation between Hg_0 and Hg_0^{-1} is 5.8 meV. Placing this value in the above equation gives a relaxation energy E_R of 8.1 meV. The value for E_R in the case of Hg_1 and Hg_1^{-1} is 14.8 meV.

Using the values for the Huang-Rhys factor determined above, one can calculate the relative intensity of the Stokes features Hg_0^{-2} and Hg_1^{-2} using *Equation (7)* where (*n = 2*). *Table 4.2.4* shows the calculated relative intensity of each of these lines, along with the determined intensity ratio based on spectroscopic measurements.

Table 4.2.4:

Line Designation	**Integrated Intensity of Peak (a.u.)**	**Intensity Ratio Relative to ZPL (Experimental)**	**Value of *S***	**Calculated Intensity Ratio Relative to ZPL**	**Discrepancy (% Experimental / Calculated)**
Hg_0	25126	-	-	-	
Hg_1	13886	-	-	-	
Hg_0^{-2}	20764	0.83	1.4	0.98	84.6%
Hg_1^{-2}	28097	2.02	2.6	3.38	59.7%

Fig. 4.2.8 is an enlargement of the Stokes sideband. The arrows point to ‘shoulders’ on these features which distort the line shape. The origin or possible relevance of these minor features is not yet established but they do not contribute significantly to the spectrum.

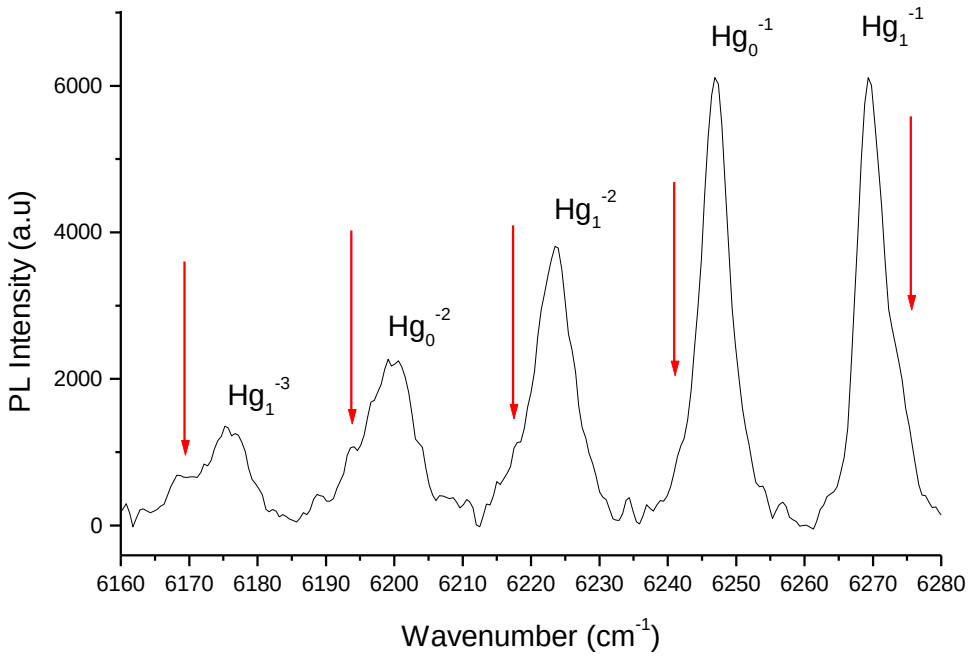

Fig. 4.2.8: Enlargement of the peaks within the phonon sideband, observed at 8.3 K. The arrows indicate evidence of overlapping peaks

Fig. 4.2.9 shows the spectrum for the ISOLDE sample at a temperature of 40.3 K. A new peak appears at 6360.9 cm^{-1} (788.7 meV), indicated by the arrow. Based on the determined phonon energy of approximately 5.7 meV, this new feature is an anti-Stokes line of Hg_1. The presence of a second peak on Hg_2 is due to the presence of an anti-Stokes line related to Hg_0

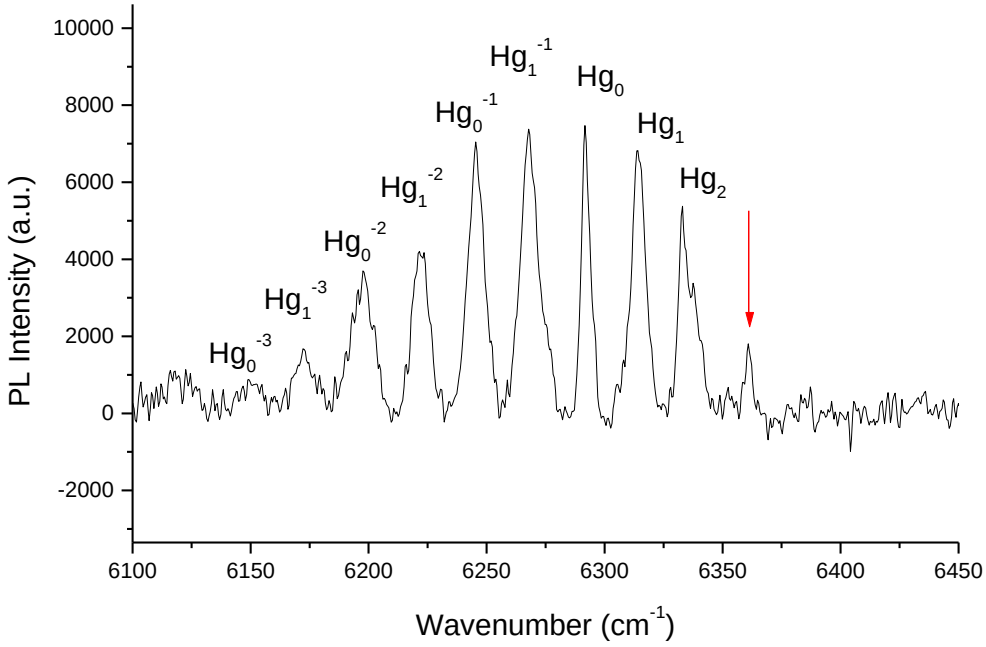

Fig 4.2.9: PL spectrum of Hg related band in ISOLDE sample at 40.3 K. A new peak is observed at an energy of 788.7 meV

4.2.3 Determination of Energy Level Structure

Fig. 4.2.10 shows the relative variation in intensity of Hg_1 with respect to Hg_0, between 3.3 and 10 K. As the temperature of the sample rises, the probability increases that a higher vibrational mode in the excited electronic state (*m > 0*) will be populated (*Section 2.2*). The intensity of an anti-Stokes line should be observed to increase for a rise in temperature. However, at such low temperatures anti-Stokes features should not be as intense as the observed lines. Therefore, this data proves that Hg_1 must be a ZPL related to a transition from the same excited state as that of Hg_0. The peak energy position is 783.1 meV which does not, to my knowledge, correspond to any previously determined element.

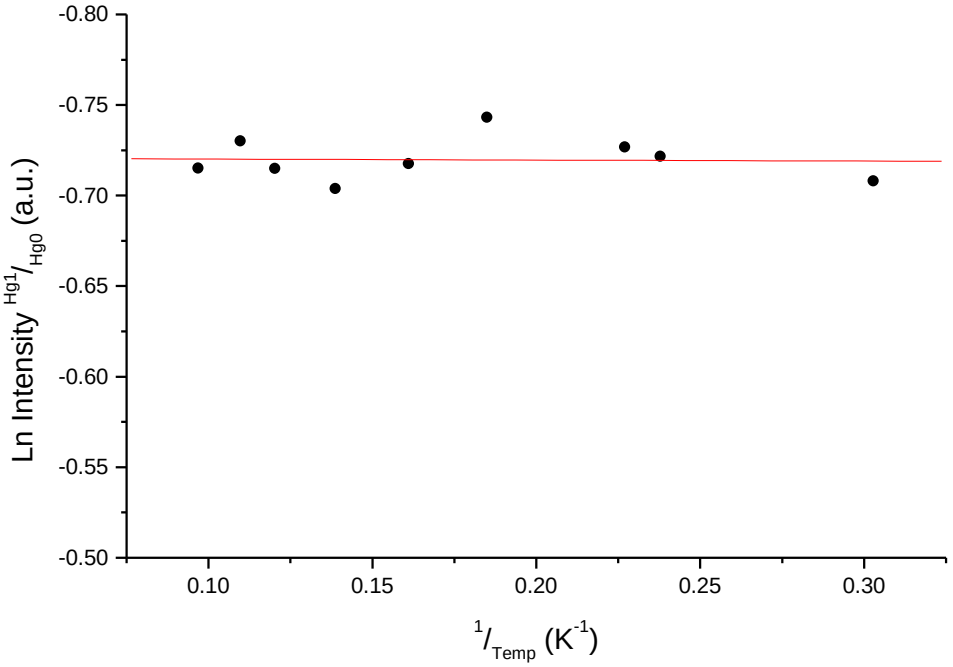

Fig. 4.2.10: Plot showing that the relative intensity of line Hg_1, with respect to ZPL Hg_0, remains constant. This confirms that peak Hg_1 is a ZPL related to a transition from the same excited state as Hg_0

Fig. 4.2.11 shows the temperature dependence of the intensity of Hg_2 with respect to Hg_0. By plotting the natural log of the intensity ratio against the reciprocal temperature, the slope of a

line fit to this data is simply $\frac{\Delta E}{k}$, where ΔE is the energy separation between the excited states of the ZPLs, and k is the Boltzmann constant. In other words, the ratio of intensity, and hence the population of the excited state, should follow a Boltzmann distribution as the temperature is increased.

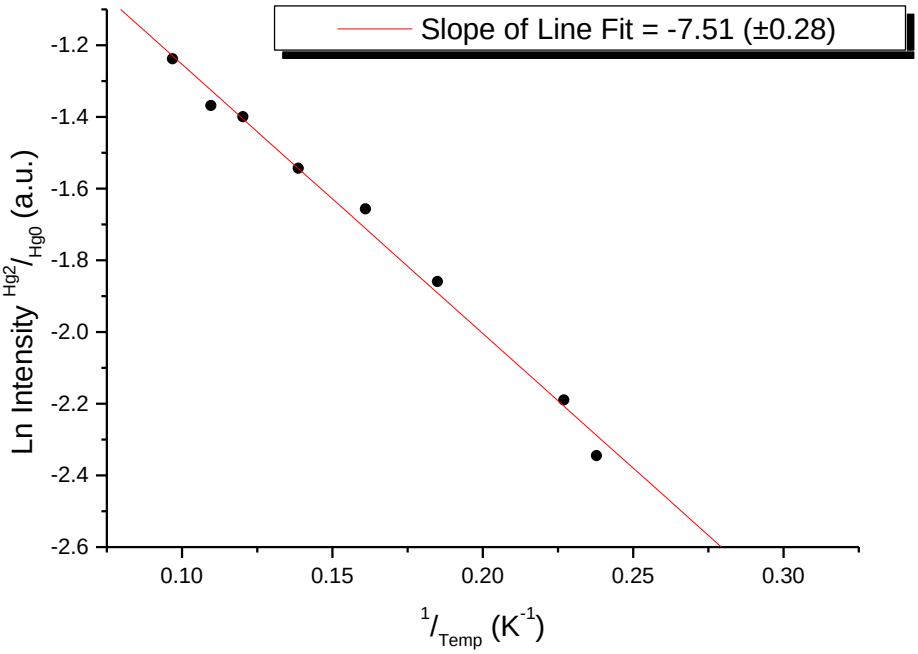

Fig. 4.2.11: Intensity ratio of line Hg_2 to ZPL Hg_0, with respect to temperature. The slope of the fit is determined to be –7.51, which corresponds to a value for ΔE of 0.7 meV

The slope of the line fit to this data is –7.51, which corresponds to a value for ΔE of 0.7 meV. On the basis of this temperature-dependency data and the observed line positions, the energy level structure can be determined. *Table 4.2.5* contains the peak energy position of each of the ZPLs for reference.

Table 4.2.5:

Line Designation	Peak Energy Position (meV)
Hg_2	785.5
Hg_1	783.1
Hg_0	780.4

Line Hg_0 corresponds to a transition from an excited state to a ground state. Since the thermal activation data (*Fig. 4.2.10*) shows no change in intensity of Hg_1 with respect to Hg_0, one can conclude that the transition for this ZPL occurs from the same excited state to a lower energy ground state. The energy separation, based on the obtained spectra, between these ZPLs is 2.7 meV (*Table 4.2.5*). This indicates that the relative energy difference between the two ground states must be 2.7 meV to account for the higher photon energy. *Fig. 4.2.11* suggests that the Hg_2 line occurs from an excited state 0.7 meV above the excited state for the other ZPLs, to a third ground level. Since the separation from Hg_2 to Hg_0 is 5.1 meV (*Table 4.2.5*) this third level must be 1.7 meV below the second to account for the energy. This structure is shown in *Fig. 4.2.12*, along with the factors *A*, related to the probability of transition and degeneracy of levels (*Section 2.2*). The values for *A* were obtained from y-axis intercepts of *Figs. 4.2.10* and *4.2.11*. It should be noted that we cannot deduce the degeneracy *g* for each level.

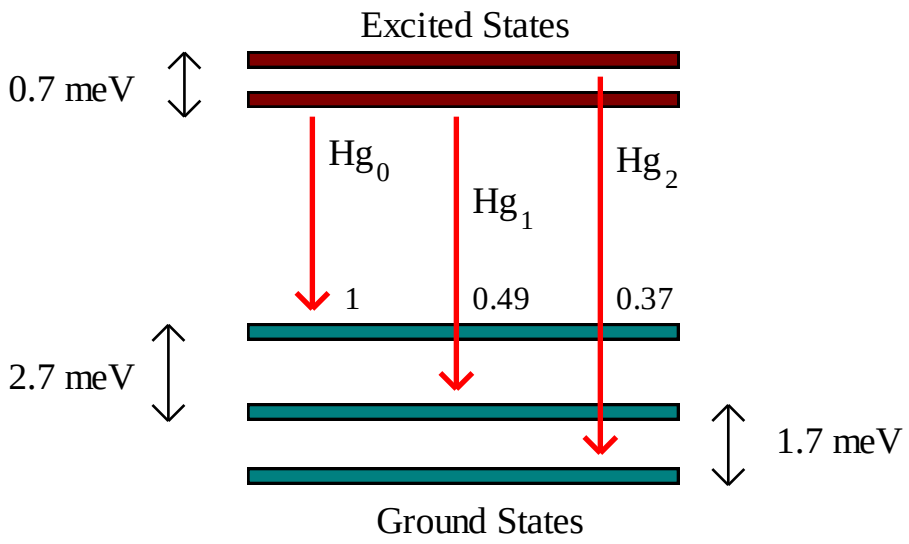

Fig. 4.2.12: Energy level structure for Hg-related defect, showing a triple ground state and double excited states. The numbers 1, 0.40, and 0.37 are values for A determined from Figs. 4.2.10 and 4.2.11

Whilst *Fig. 4.2.12* is sufficient to explain the origin of each of the ZPLs, there are a number of transitions that could also occur within this structure. These are illustrated in *Fig. 4.2.13*.

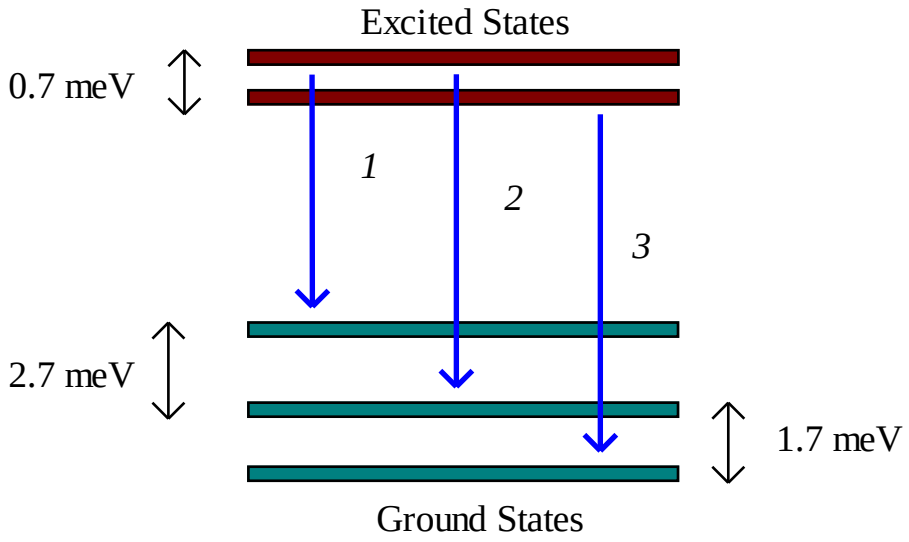

Fig. 4.2.13: Transitions within the determined structure that do not correspond to the observed ZPLs

Transitions labelled (*1*) and (*2*) would occur from the higher excited state of the defect. These would correspond to PL peaks with an energy just 0.7 meV (5.6 cm^{-1}) higher than Hg_0 and Hg_1 respectively. However, since transition (*3*) would occur from the first excited state, it would correspond to a PL line at an energy 0.7 meV below that of Hg_2. *Fig. 4.2.14* is an enlargement of these ZPLs, as observed in the ITEN sample at 4.4 K illustrating that there is spectral evidence for some, but not all, of these transitions. Whilst there is evidence for transitions *1* and *2*, there does not appear to be evidence for *3*. This could simply be due the line intensity being very weak and indistinguishable from background noise. In any case, the model presented here for the energy level structure does explain the origin of each of the ZPLs, and correctly predicts the location of two additional peaks. It is submitted as a tentative attempt to explain the line structure.

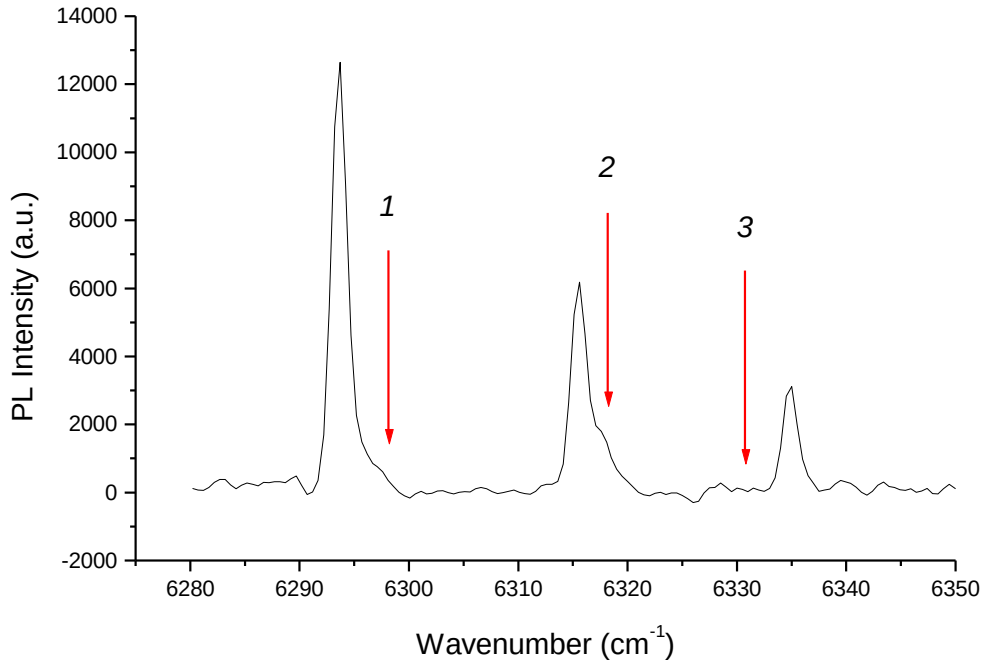

Fig. 4.2.14: Enlargement of each of the ZPLs as observed in the ITEN sample at 4.4 K. Whilst there is spectral evident of transitions 1 and 2, there is no evidence for transition 3 in the expected region

4.2.4 Radioactive Decay Data and Determination of Defect Identity

During the previous discussions, the broad band observed in both ITEN and ISOLDE samples was attributed to Hg. The reasons for this assignment shall be discussed in this section. Both p- and n-type silicon samples, implanted with ^{197}Hg at ISOLDE, have been found to contain this same band. The decay path for ^{197}Hg is:

$$^{197}_{80}Hg \xrightarrow{64.1h} ^{197}_{79}Au \text{ (stable)}$$

where the half-life of the decay is 64.1 hours. *Fig. 4.2.15* shows the change in intensity of the 780.4 meV line (designated Hg_0 above) with respect to time, of a p-type FZ sample implanted with ^{197}Hg to a concentration of 2×10^{12} atoms cm^{-2}. The delay of nearly 40 hours between annealing and first PL examination was due to this particular sample being but one of eight obtained. On the basis of spectroscopic measurements within that 40 hour space, it was decided to follow the decay of the feature in this sample rather than the others.

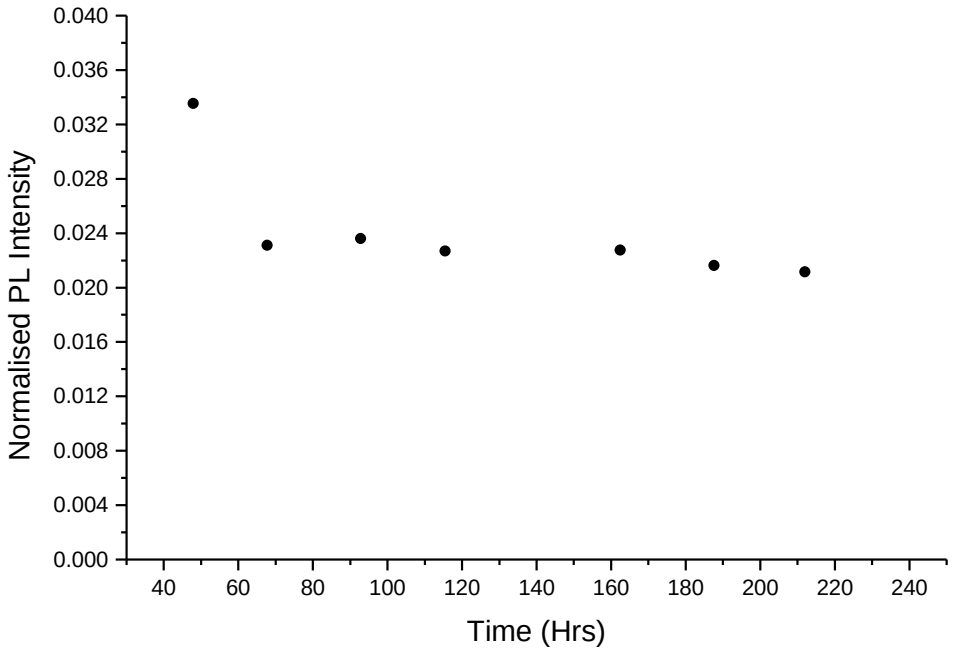

Fig. 4.2.15: Intensity versus time plot for the 780.4 meV ZPL The x-axis is, in this case, the time after the annealing step

However, this data is entirely inconclusive because the intensity reduces by less than a factor of 2 over the time interval and appears linear. Fortunately, Henry *et al.*[1] previously conducted experiments that indicate the defect could be related to single Hg atoms. ^{197}Hg was implanted into n-type Si material at the ISOLDE facility and the intensity of the feature was observed to decay with a half-life time fitting approximately 68 hours - close to the 64.1 hour decay from ^{197}Hg to ^{197}Au (*Fig. 4.2.16*). This is, in my opinion, a strong indication of the involvement of Hg although we cannot, at this stage, rule out the involvement of some other element in conjunction with Hg.

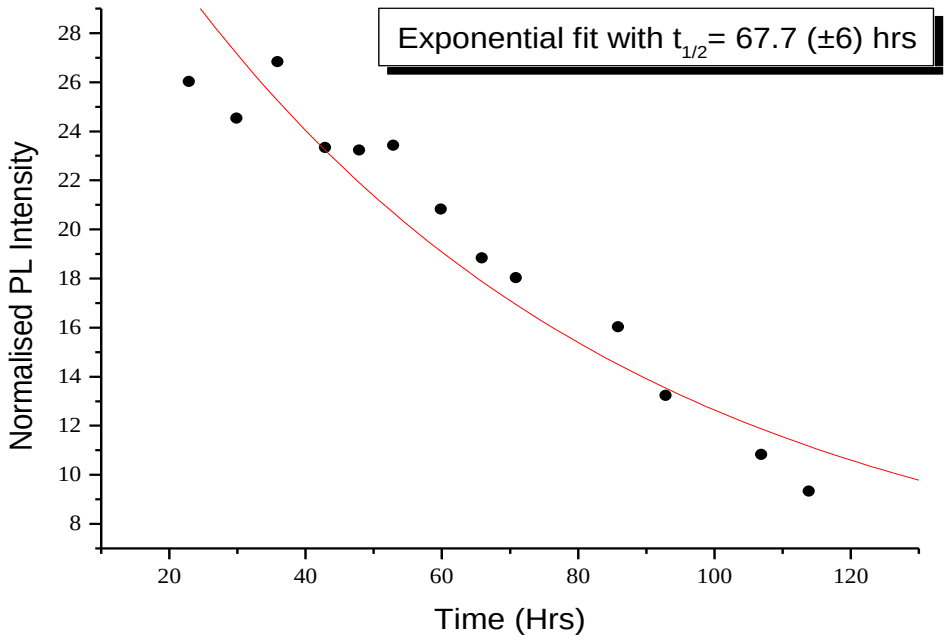

Fig. 4.2.16: Graph obtained previously by this group[1], also illustrating that the rate of decay of the observed defect is consistent with that of ^{197}Hg

It is important to note that the defect has not previously been reported by other groups, and has appeared in approximately 20 samples, each implanted with one of four isotopes of Hg (masses of 193, 197, 200 and 203). Since the intensity of the feature is extremely high, it seems doubtful that it could be due to another element (or elements) and yet not been observed before. Whilst not conclusive proof of the identity, it does suggest that the defect is related to some element introduced during implantation of Hg. The ITEN sample does not contain defects related to Pt, so one can rule out that possible assignment. Tl contamination could be a factor in the production of the defect, but γ-ray spectroscopy has shown that the ratio of Tl to Hg concentrations at the ISOLDE facility is approximately 1:100 respectively, for ^{197}Hg. It is unlikely, therefore, that Tl is a major contributor to the defect.

The determined value of approximately 5.7 meV for phonon energies does suggest the involvement of a high-mass defect centre. From tabulated data given by H. Conzelmann, the vibrational energy for a defect involving ^{197}Au was experimentally determined to be approximately 3 meV, calculated in theoretical models to be 4.4 meV[5]. The 5.7 meV value given here is therefore consistent with the known properties of high-mass interstitial transition metals.

4.2.5 The ‘x’ Band

Many of the samples implanted at ISOLDE with ^{197}Hg and ^{200}Hg, as well as the samples implanted with ^{200}Hg at ITEN, revealed a small group of lines that have been labelled as ‘*x*’ in the following discussion. *Fig 4.2.17* shows this defect for the ^{200}Hg ITEN-implanted Si, at 3.3 K. It consists of a number of narrow lines with a separation of approximately 4.8 meV. The highest energy line in the group, at 6708.2 cm^{-1} (831.8 meV), is probably a ZPL.

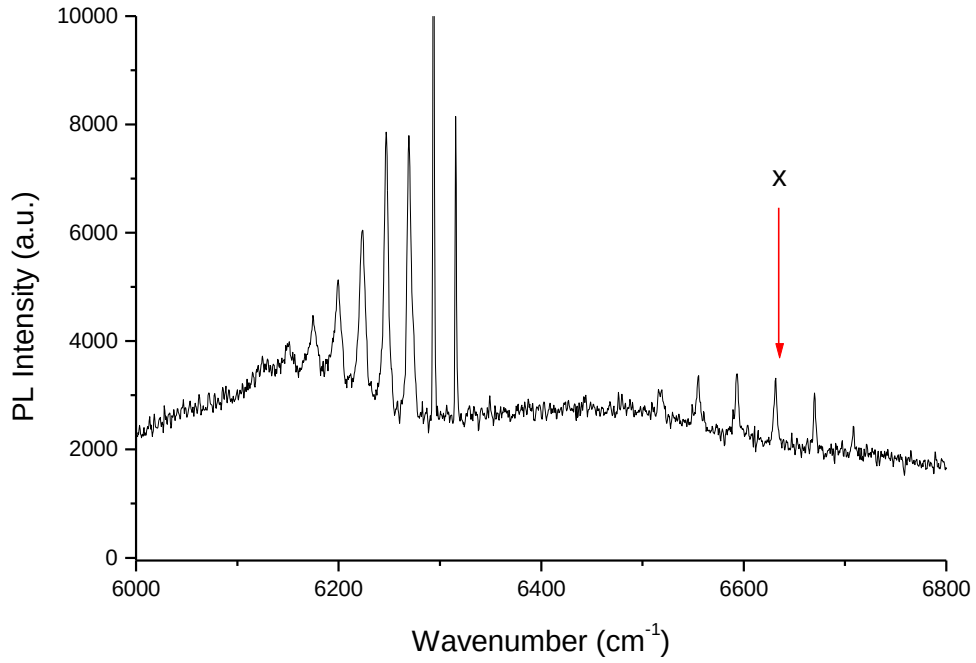

Fig. 4.2.17: Examination of ITEN sample implanted with ^{200}Hg at 3.3 K revealing a small band which has not previously been reported. The broad band extending from approximately 6100 to 6400 cm^{-1} is the Hg-related feature discussed above

Fig. 4.2.18 shows the same spectral region for the sample implanted with ^{200}Hg at the ISOLDE facility. As can be seen, this sample also contains the newly observed defect.

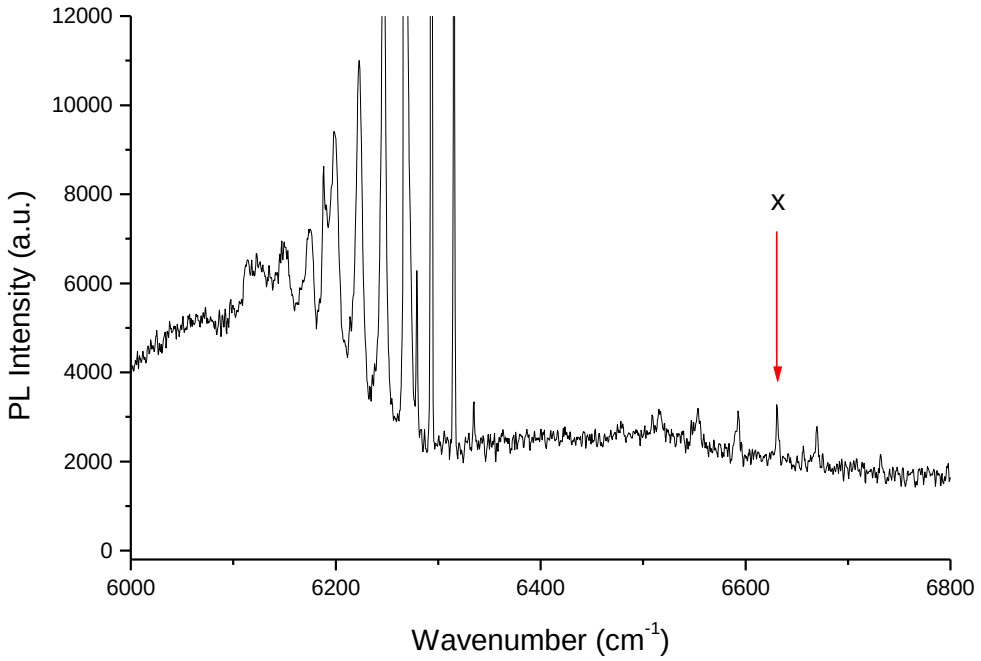

Fig 4.2.18: Examination of ISOLDE ^{200}Hg sample at 3.7 K revealing the 'x' band and the broad Hg-related feature discussed above

This feature has, to my knowledge, not been reported previously. Its behaviour is somewhat unusual in that it is barely discernable from background noise at temperatures above approximately 4.8 K, as shown in *Fig. 4.2.19* for the ISOLDE sample. The results presented here were taken a year after the initial implantation, indicating the band is stable despite room temperature storage. It is suggested that it is related to atoms introduced by the implantation equipment rather than impurities present in the starting material. This would limit the identification of the defect to being Hg- or Au-related, or possibly the result of Tl contamination. It is almost certainly not Pt-related because it appears in ITEN samples that show no evidence of other Pt lines. The identity might be established by performing PL measurements below 4 K on samples implanted with radioactive Hg ions. To date, examinations of the broad Hg-related defect described above have occurred at higher temperatures than this because it remains relatively unchanged at temperatures to around 10 K. This is the reason, I believe, it has been previously missed. Since the new defect appears in samples more than a year after initial implantation, problems associated with thermal dissociation are irrelevant so longer lived isotopes could conceivably be used.

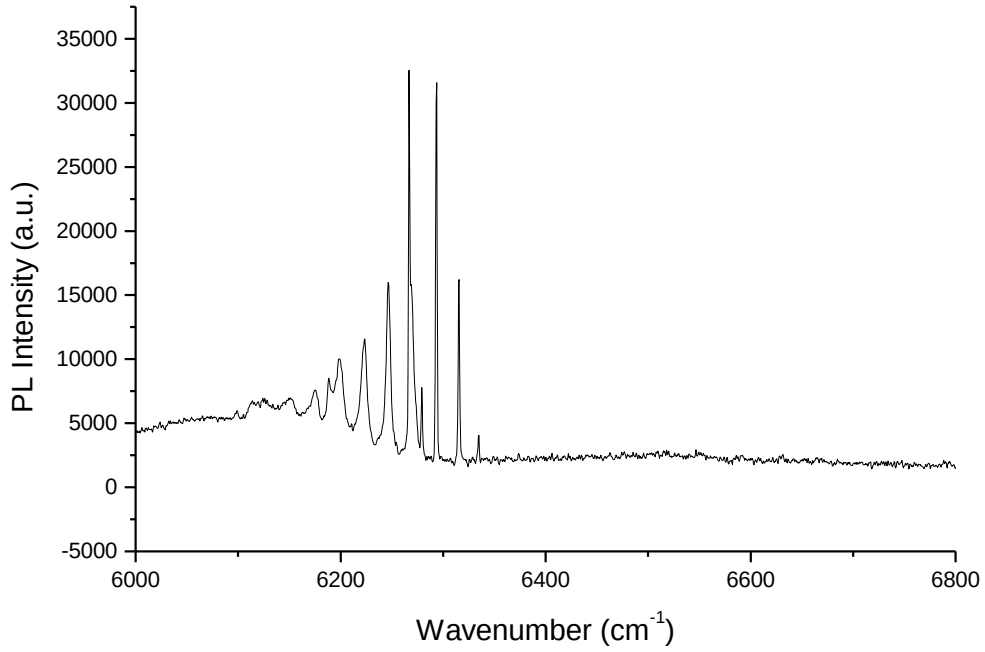

Fig. 4.2.19: ISOLDE sample examined at 4.8 K. The small feature referred to as 'x' above is barely discernable from the background noise

The temperature behaviour of the 'x' band is similar to that of defects with metastable states, such as Tl and In[6]. In these cases, defect atoms have two lattice configurations and heating of samples causes the defect to switch from one to the other, revealing new spectroscopic features at the expense of others. One possible explanation for the observed behaviour of the 'x' band is that it similarly has two configurations, the second of which is not optically active.

4.3 'FeB'-Related Defect

Electron Paramagnetic Resonance (EPR) experiments conducted in the early 1960's by Ludwig and Woodbury, revealed a defect which was assigned to a trigonal FeB complex[1]. In 1982, R. Sauer and J. Weber performed PL measurements on Fe-doped Si and observed a number of spectral features between 1000 and 1080 meV that were largely believed to be due to 'FeB' defects[2]. One of the designated Zero Phonon Lines (ZPL), appearing at 1066.8 meV, was labelled FeB_1^0 accordingly, and was correlated to the defect discovered by the earlier EPR measurements.

Sauer and Weber's paper was influential in establishing the chemical identity of these defects because the 'FeB' lines had not only been observed in material into which Fe was diffused, but also in Si where Fe and B had been added to the melt during the crystal growth process. The researchers were able to correlate their data to DLTS measurements where varying concentrations of the constituent atoms were used[3], and offer a recombination model based on the original EPR observations.

The following year, however, Mohring, Weber and Sauer published a paper indicating that their luminescence data was 'inconsistant with an identification of the optical centre with FeB pairs'[4]. This was due largely to the belief that the spectroscopic lines were too intense for their estimated 10^{11} cm^{-3} concentration of traps. Ludwig and Woodbury's EPR experiments showed that 'FeB' centres were highly anisotropic, but Zeeman measurements by Mohring *et al.* failed to correlate with this assignment. Schlesinger *et al.*[5] failed to observe line shifts in the 'FeB' defects after Fe isotope substitution, and annealing studies performed by Klugge *et al.* showed that the 1067 meV line could not be due to trigonal FeB[6].

In 1996, Henry *et al.* performed an experiment at the ISOLDE facility and implanted ^{193}Hg into silicon samples[7]. The dosages used were of the order of 10^{12} atoms cm^{-2}, and the decay series for this particular isotope is:

$$^{193}Hg \xrightarrow{4h} {}^{193}Au \xrightarrow{17.7h} {}^{193}Pt(stable)$$

When the PL spectra were observed, Henry *et al.* noted a decrease in intensity of the 1067 meV 'FeB' line over a period that seemed to correlate with the 17.7 hour decay from Au to Pt. This

graph is shown in *Fig. 4.3.1*, and is fairly conclusive proof that the 'FeB' defect is not related to Fe, but is instead related to Au.

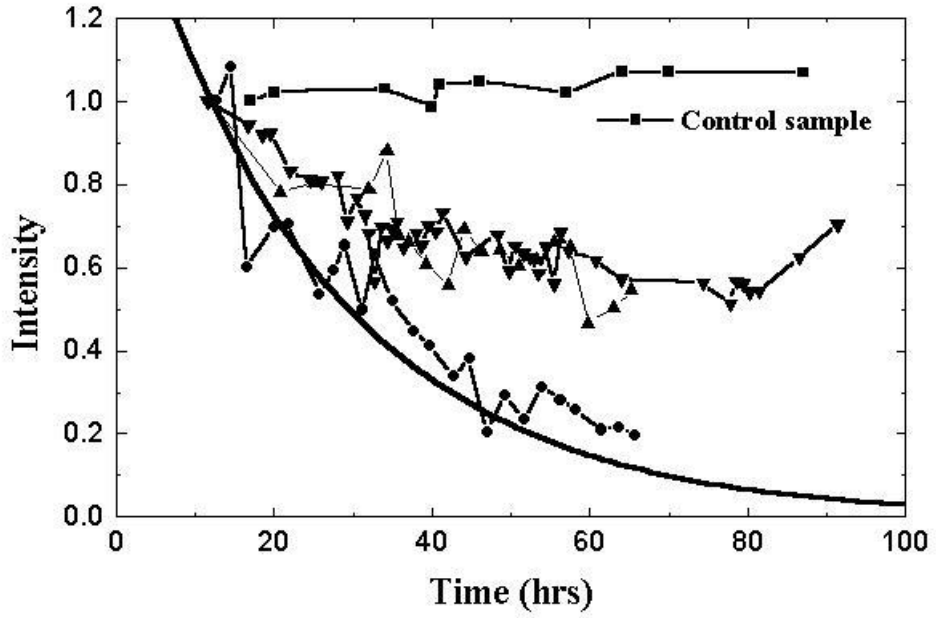

Fig 4.3.1: Intensity versus time plot for samples implanted with ^{193}Hg obtained by Henry et al.[7]. The control sample shows little change in intensity, whilst the implanted samples decrease in intensity. One sample decays with a half-life close to that of the transition from Au to Pt. The sample data which does not match this decay rate, is due to the presence of some stable Au in the sample

For my experiments I wished to corroborate this result. Due to experimental constraints and the need to ship radioactive samples from the ISOLDE facility to spectroscopic equipment, ^{193}Hg was not ideal because of the relatively short half-life times. Therefore ^{197}Hg was chosen because it decays to stable ^{197}Au and has a relatively long half-life of 64.1 hours. Unlike the previous experiments, one would expect the intensity of a Au-related 1067 meV line to increase over time as more of the Hg decays to Au.

Figs. 4.3.2 and *4.3.3* show regions of the PL spectrum of ^{197}Hg implanted p-type Si shortly after annealing. The dosage used was 2×10^{12} atoms cm^{-2}, and the samples were prepared and annealed as described previously. The 1067 meV (8404 cm^{-1}) line under investigation is labelled '*FeB*', and descriptions of other lines can be found in *Table 4.3.1*.

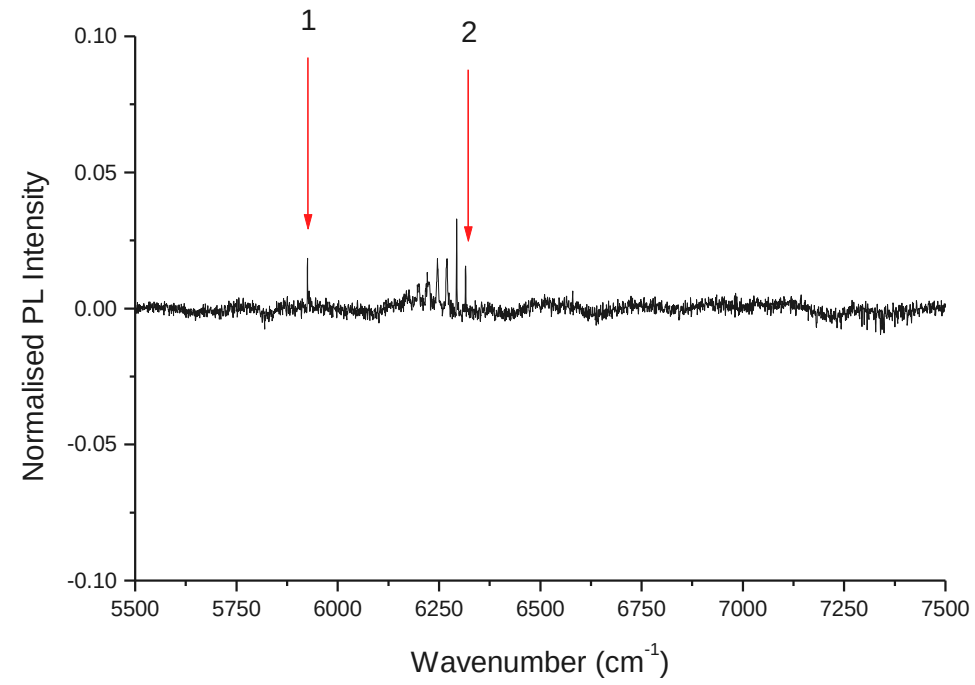

Fig. 4.3.2: PL spectrum of p-type Si implanted with ^{197}Hg shortly after annealing

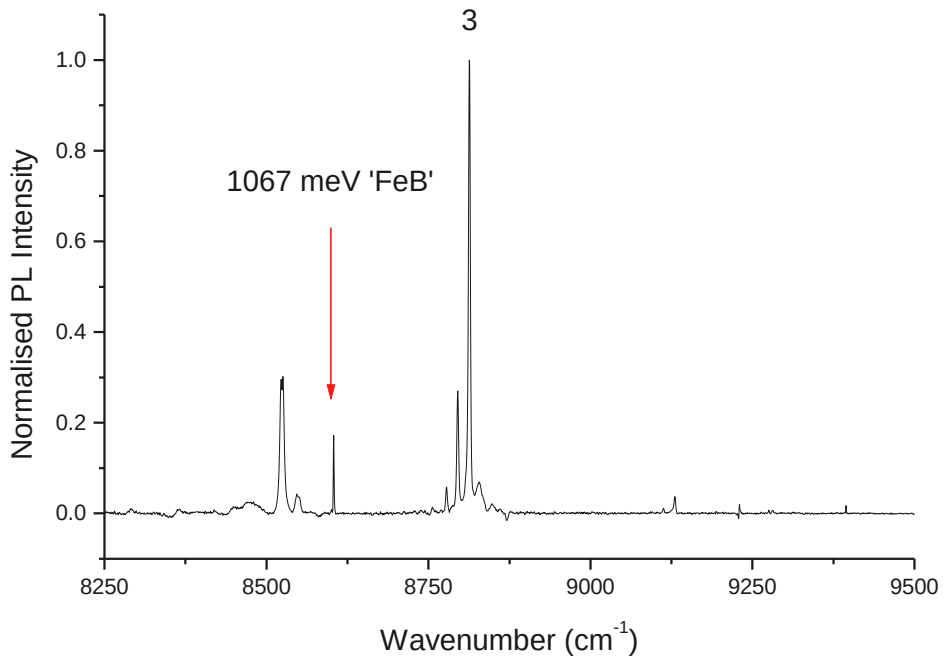

Fig. 4.3.3: PL spectrum of the same sample implanted with ^{197}Hg. The 1067 meV 'FeB' line is indicated by the arrow, and the features at lower energy are other 'FeB'-related centres described in the references given previously

Table 4.3.1:

Designation	Identification
1	*Au-Fe related peak (735 meV) described by Henry et al.*[8]
2	*Hg-related band described in Section 4.2*
3	*Boron-related bound-exciton line*

The intensity of the 1067 meV line was observed over time, and its intensity was found to *decrease*, not increase as expected. *Fig. 4.3.4* shows a comparison of the spectrum of this line as obtained at two different times.

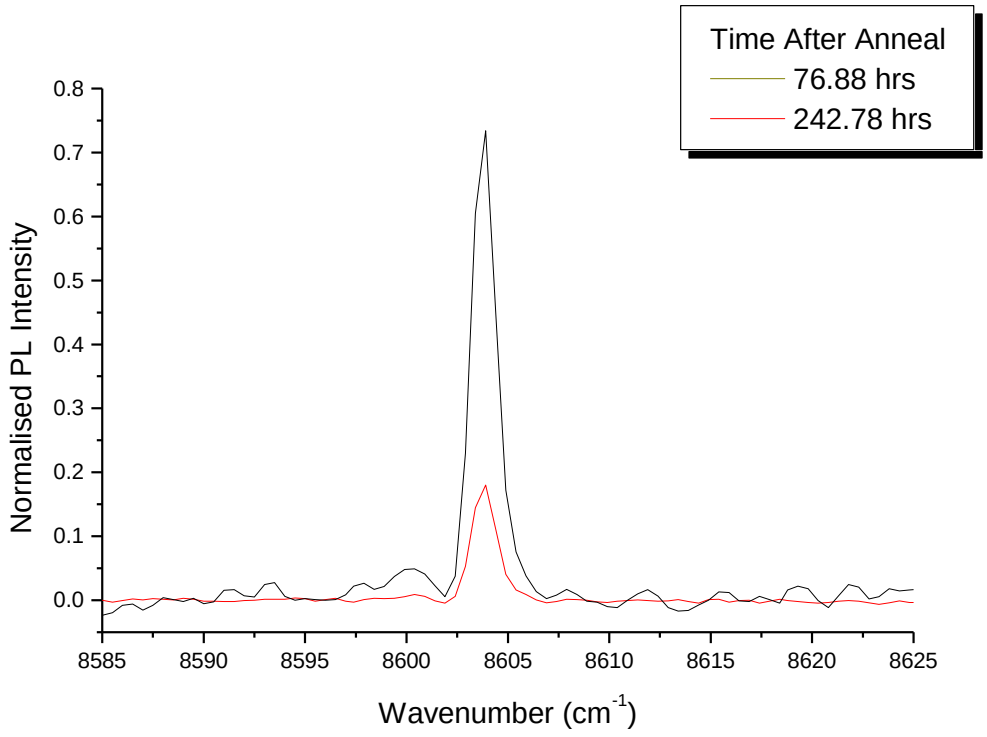

Fig 4.3.4: Illustration of the change of intensity with respect to time of the 1067 meV line

When I fit an exponential decay to the intensity versus time data points (*Fig. 4.3.5*), the resultant curve suggested that the defect decays with a half-life of some 70.3 hours – close to the 64.1 hour half-life of the Hg transition to Au!

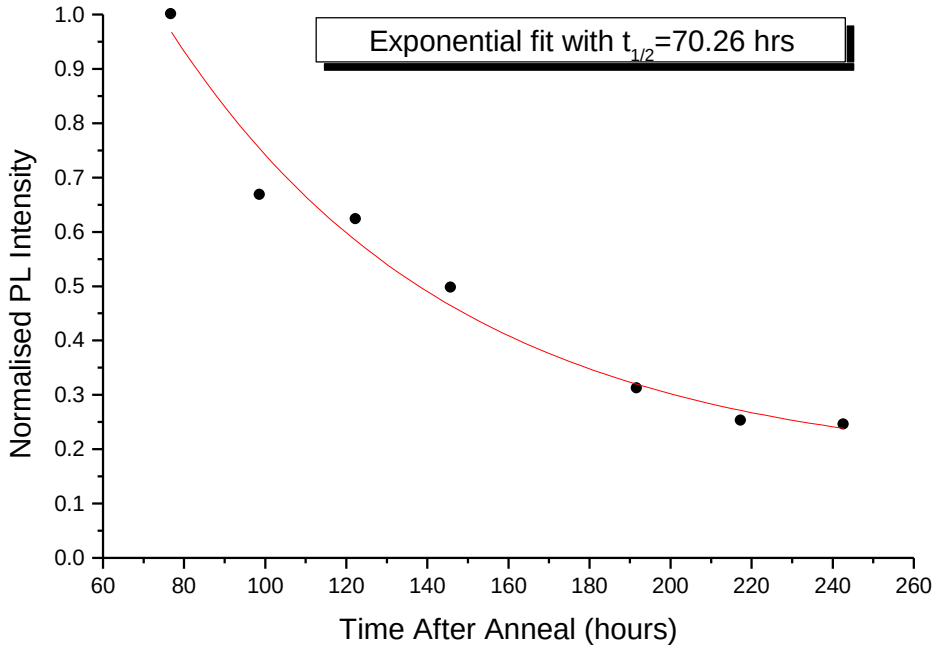

Fig. 4.3.5: Exponential fit to intensity versus time data for the 1067 meV line. The value of approximately 70 hours is close to the half-life of the decay from ^{197}Hg to ^{197}Au (64.1 hrs)

There are two possible explanations for this:

The first is that the 1067 meV 'FeB' feature is not related to Au but Hg instead. Whilst this could explain the observed decrease in line intensity, it contradicts the previous study performed using radioactive Hg/Au which established the involvement of Au.

The alternative explanation, evidence for which shall be discussed below, is that some other process destroys the Au-related defect at a faster rate than it is created by the radioactive decay from Hg. In order to obtain information regarding this rate, it was decided to model the intensity changes of the 1067 meV line *as if the Au end-products were not stable*. The decay would therefore be a two-stage process - Hg decaying to Au creating the radiative defect, then Au to some other state which would destroy it. We do not imply a radioactive decay for Au, rather that the Au defect produced by the decay of Hg is unstable.

The equation describing the number of Au atoms N_{Au}, related to the intensity of the PL peak, for this decay process is:

$$N_{Au} = c\left(\frac{\lambda_1}{\lambda_2 - \lambda_1}\right)\left(e^{-\lambda_1 t} - e^{-\lambda_2 t}\right)$$

(11)

where *c* is simply a scaling constant, λ_1 is the decay constant of Hg to Au which creates the defect, λ_2 is the decay constant for the destruction of the defect, and *t* is the time elapsed after the anneal. The decay constant is related to the half-life $T_{1/2}$ by:

$$\lambda = \frac{\ln 2}{T_{1/2}}$$

(12)

Since λ_1 can be calculated from the known half-life of 64.1 hours, by fitting the values of *t* and N_{Au} to the intensity versus time data in *Fig. 4.3.5* one can determine the value of λ_2 that is required to produce the observed decay of 70.3 hours. *Fig. 4.3.6* shows this curve fit.

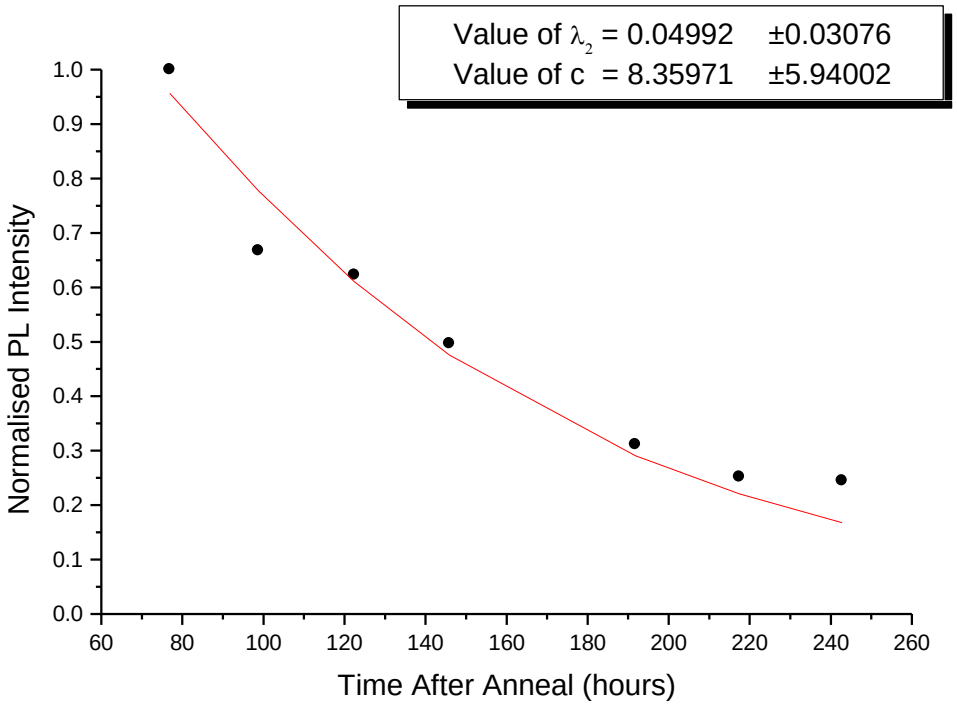

Fig. 4.3.6: Curve fit of two step decay equation to intensity data of 1067 meV line. It suggests that the rate at which the defect is destroyed has a decay constant of approximately 0.05 hr^{-1}

The calculated value for λ_2 is 0.0499 hr^{-1} which corresponds to an equivalent half-life of nearly 14 hours. The errors in this determination are very large, with a maximum value of this half-life being some 36 hours. Since γ-ray measurements, as described in *Section 3.2.2,* confirmed the presence of ^{197}Hg in the samples, one can be certain that the final decay product is stable Au. Although the above curve fitting determines the rate of destruction of the defect, one must explain this in terms of some phenomena other than radioactive decay.

One possibility is that the defect is thermally dissociated as a result of storage at room temperature between measurements. Sauer and Weber, in their 1982 paper[2], indicate that the 'FeB' luminescence spectrum 'is gradually obscured by other PL bands upon room temperature storage for some days'. This is certainly consistent with the calculated destruction rate using the decay model above. In their later paper, Mohring *et al.*[4] provide an expression for the dissociation time of the 'FeB' defects:

$$\tau = 3.7 \times 10^{-11} \exp(0.92eV / kT)$$

where τ is the dissociation time in seconds. If one assumes a room temperature of 293 K, the calculated dissociation time is 2.7 days. The 14 hour value calculated for the decay constant results in less than 5% of the Au remaining in the defect after a 2.7 day period. Clearly these low quantities of Au suggest the modelled decay rate is of the right order of magnitude to be consistent with the known dissociation behaviour of the 'FeB' defect.

Although the results presented here are insufficient to conclude the defect being related to Au, I have been able to offer an explanation for this failure which does not require one to dismiss data previously obtained by radioactive isotope implantation. In the case of these earlier experiments, the isotope implanted had a relatively short half-life, which enabled the samples to be maintained at liquid helium temperatures for the duration of examination. The use of radioactive ions led to a correction of the mistaken identification of this defect, and illustrated the usefulness of the technique. However, this study indicates that thermal dissociation of radioactive defects is an important consideration, and could lead to misidentifications of their chemical identity.

4.4 AuLi-Related Defect

Previous work had identified a new PL defect which appears at approximately 1004 meV. The initial results below are taken from Henry *et al.*[1]. ^{193}Hg was implanted into p-type FZ Si wafer pieces at the ISOLDE facility in concentrations of the order of 10^{12} atoms cm^{-2}. The decay series for ^{193}Hg is:

$$^{193}Hg \xrightarrow{4h} {}^{193}Au \xrightarrow{17.7h} {}^{193}Pt(stable)$$

Li was diffused into the samples by placing small amounts of the metal in the ampoule during the annealing process, as described in *Section 3.3*. Photoluminescence data was gathered at 4.2 K, revealing the new defect at 1004 meV. The intensity of this line was assessed over time and the defect was found to decay with an effective half-life of some 8.0 ± 0.5 hours (*Figs. 4.4.1* and *4.4.2*).

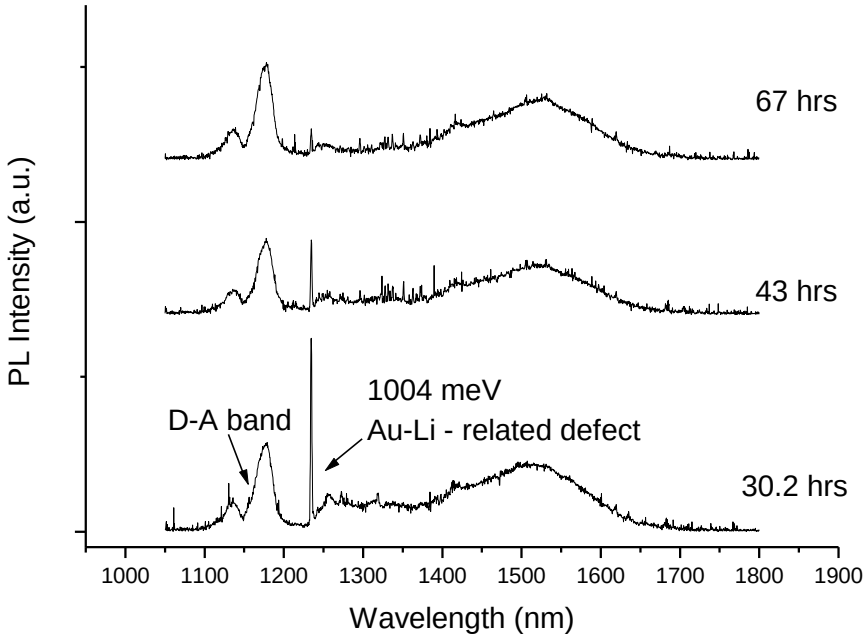

Fig. 4.4.1: PL spectra illustrating the decrease in intensity over time of the 1004 meV defect obtained by Henry et al.[1]. The 'D-A' band is due to donor-acceptor recombinations, involving Li donors and the B acceptors in the starting material. The time intervals relate to the lapse of time since the annealing process

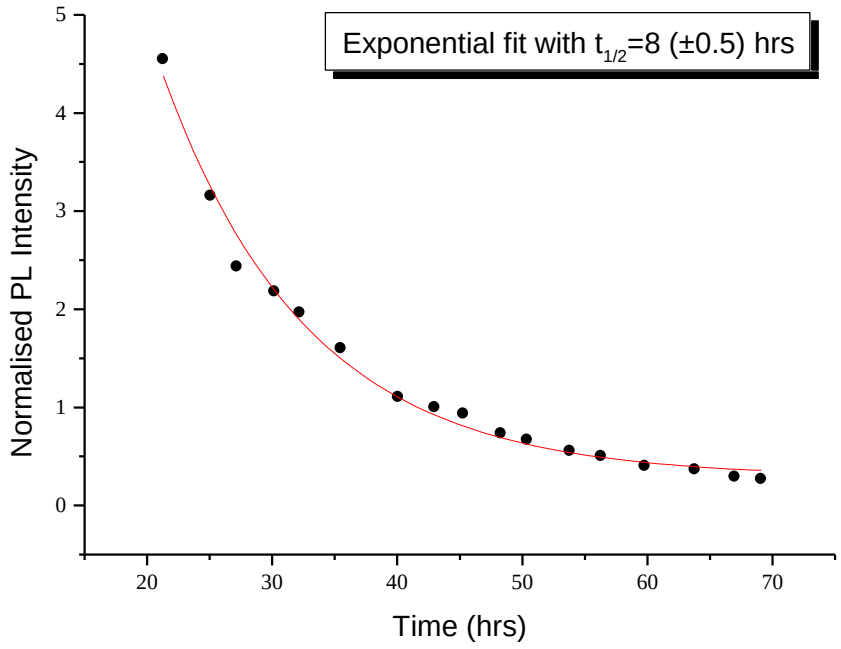

Fig. 4.4.2: Intensity versus time plot for the 1004 meV line based on data obtained by Henry et al.[1], showing it to decay with a half-life of 8 hours. This suggests the decay is related to a pair of Au atoms – the half-life of 17.6 hours for a single Au atom reducing by a factor of 2 for the pair

Since the decay from ^{193}Au to ^{193}Pt has a half-life of 17.7 hours, about double the observed decay rate, this suggests that the defect is related to a centre involving a pair of Au atoms. It has not, to my knowledge, been reported previous to this. The 1004 meV line has only been observed in p-type material and has not been reported for either Hg or Au implantation[2] or in cases where Au was diffused into Si. One can conclude that the defect is created as a Hg pair with the Li either incorporated in the complex, or acting as a catalyst for defect formation.

It was decided to implant ^{197}Hg into Si in equivalent concentrations and to diffuse Li into the samples as before. The decay series of ^{197}Hg is:

$$^{197}Hg \xrightarrow{64.1h} {}^{197}Au(stable)$$

Fig. 4.4.3 shows the observed PL spectrum shortly after annealing, revealing the new defect. Due to the time taken for transport from the implantation facilities to spectroscopic equipment, the samples already contained appreciable quantities of Au. The actual peak-energy position of the line of

interest is 1004.0 ± 0.1 meV. The identification of other spectral features is given in previous sections.

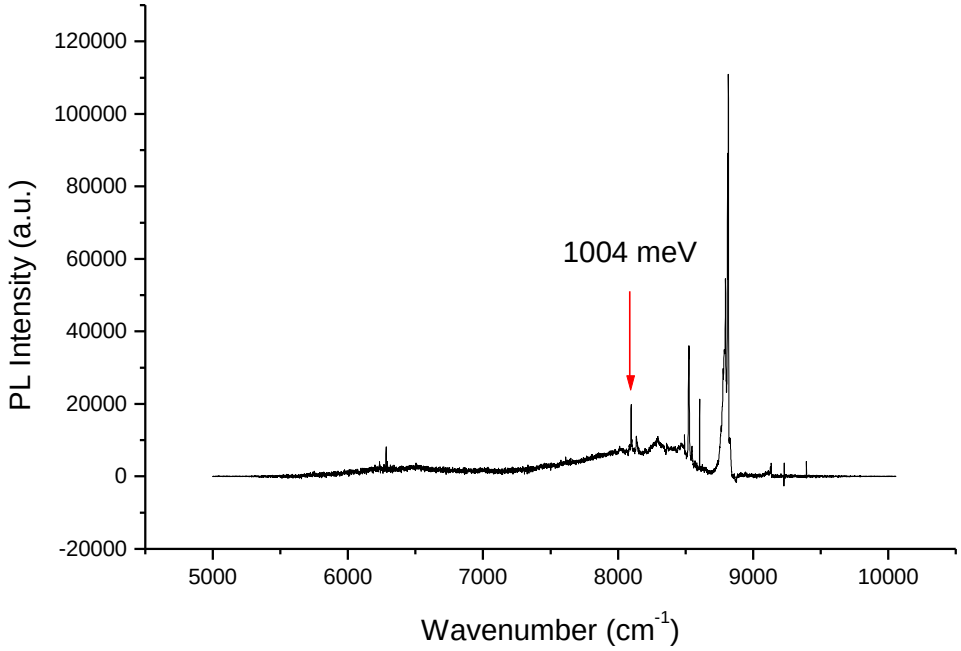

Fig. 4.4.3: PL spectrum for p-type Si sample implanted with ^{197}Hg. Li was diffused into this sample, and the 1004.0 meV line observed

Fig. 4.4.4 shows the time dependence of this defect, the x-axis here referring to the elapsed time after annealing, and indicates a decay half-life of approximately 70 hours. This is entirely inconsistent with the assumed behaviour. If related to Au, the intensity of this peak should increase, not decrease as shown. Interestingly, this graph indicates that some process is destroying the Au-Li complex at a rate similar to that of the 'FeB' defect (involving Au) discussed above. This would suggest that migration of Au at room temperature could be involved in both defects.

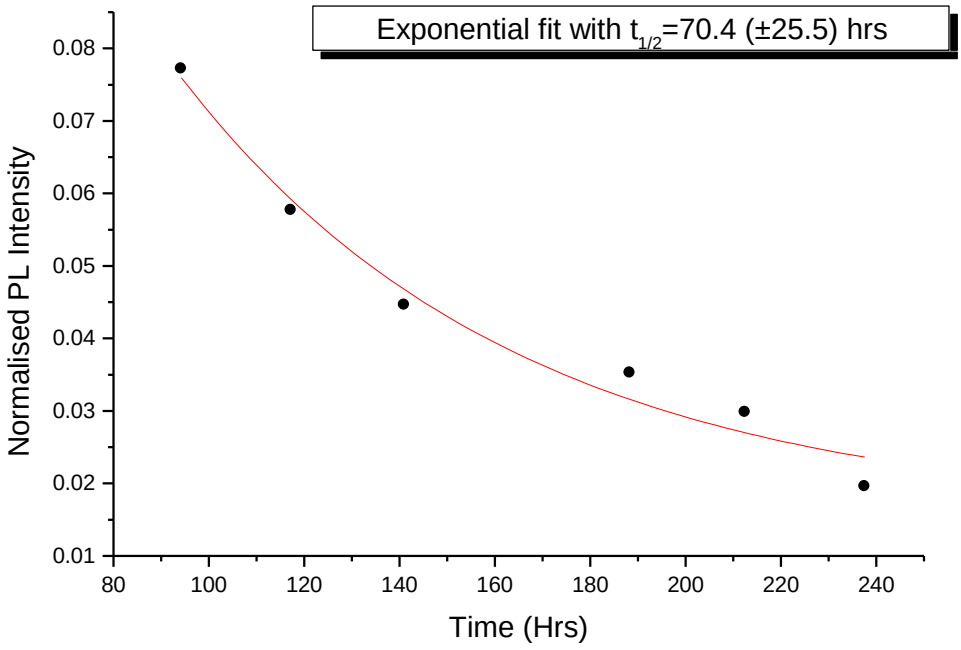

Fig. 4.4.4: Time dependence of 1004 meV defect. The decay is entirely inconsistent with an identification of the defect with Au-Li. This is, I suggest, due to thermal dissociation of the defect as in the case of the 'FeB' defect discussed previously

The results presented here cannot confirm the assigned chemical identity of the 1004.0 meV line. Nevertheless, it is included because it indicates the techniques necessary to produce the observed line, and to provide confirmation that it can be created at will should future investigations be undertaken. The feature has only been seen in samples diffused with Li – there is no evidence of the line in more than twenty samples containing only Hg. Although not conclusive, this does indicate the necessity of Li for its formation. That it should only appear in Hg-implanted samples that decay to Au strongly suggests the involvement of Hg/Au in the complex. Clearly one must minimise the length of time after implantation that the spectroscopic measurements take place, so that thermal dissociation does not become a factor that negatively influences the intensity of lines.

4.5 Si:Ge Quantum Well Structures

Fig. 4.5.1 is a diagram illustrating the energy configuration of two semiconductor materials with different bandgap widths brought into contact with one another. Such a structure is known as a *heterojunction*. At the contact regions, steps in energy bands appear which can confine carriers and can be treated as the walls of a quantum well. The levels labelled *E1* and *E2* are available energy states within this well.

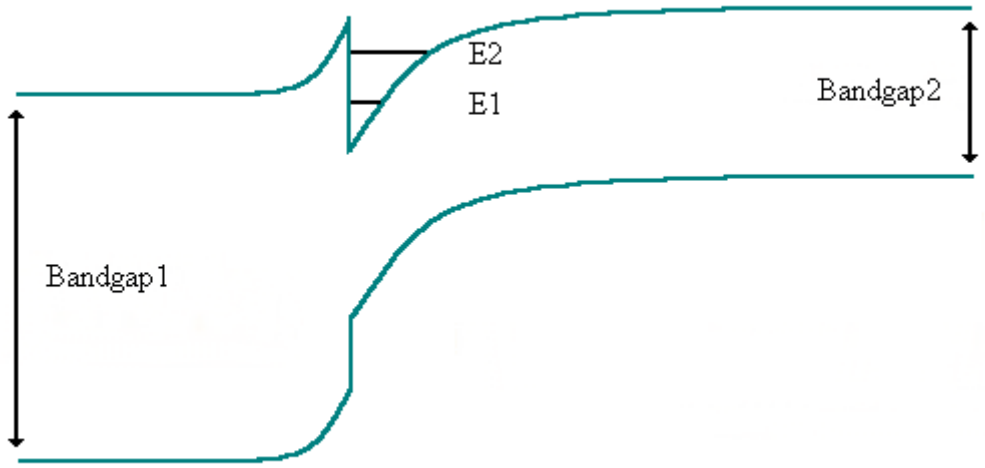

Fig. 4.5.1: The formation of a heterojunction by joining two semiconductor materials with different bandgap energies

At regions far from the interface the two semiconductors must be electrically neutral. The position of the Fermi level in each material is dependent on the doping concentration, so if there is to be no net electron transport in the absence of a bias voltage, these levels must coincide throughout the semiconductors. If one were to join two heterojunctions together, and decrease the width of the narrow-gap layer, as illustrated in *Fig. 4.5.2* a *quantum well* is formed.

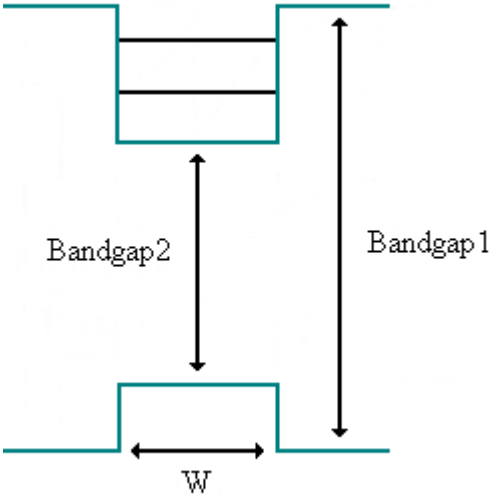

Fig. 4.5.2: As the narrow-gap layer decreases in width, a rectangular 'quantum' well is formed

For a number of applications, many-layered heterostructures with periodically repeating wells are grown (*Fig. 4.5.3*).

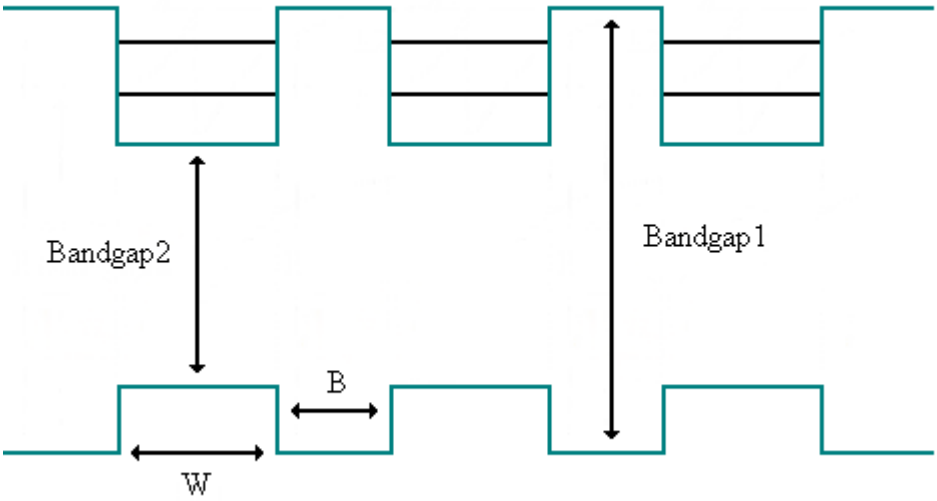

Fig 4.5.3: A periodic system of quantum wells

In the figure above, *B* is the width of the wide-gap layers. If the value of *B* is sufficiently small (typically of the order of <100 Å) charge carriers can tunnel between wells, transforming the discrete energy levels into bands. For larger wide-gap layer widths, the carriers remained confined to individual wells and an amplification of the effects of a single well is observed. Clearly, in order to produce high quality multi-quantum well (*MQW*) structures one must use two semiconductor

materials with similar lattice constants. If the materials are mismatched then one would expect a high density of dislocations near the interface, which could deteriorate the junction quality and prevent the observation of quantum effects.

During the course of my study I had the opportunity to perform PL measurements on MQW structures involving Si and Ge. Si has a lattice constant of 5.43 Å and bandgap energy of 1.17 eV at 0 K, whilst the constant for germanium is 5.65 Å, with a bandgap energy of 0.74 eV at 0 K. These values for the lattice constant correspond to a match between materials of 96%, which for MQW structures is a considerable difference. Through the use of other materials for MQWs, such as GaAs-$Al_xGa_{1-x}As$, a lattice match of more than 99% can be achieved[1]. One might therefore expect Ge layers on Si to be strained, and the PL of such structures to reveal dislocations. Since multi-well systems are grown on a substrate, in this case Si, the purity of this bulk material must be sufficiently high to prevent the appearance of dislocations and defect-related luminescence lines obscuring those related to the quantum structures themselves.

Three different types of samples were examined using the 514 nm Argon line at a laser intensity of 200 mW unfocused on the sample surface. The cryostat temperature, measured at the heat exchanger, was approximately 4.2 K for each. The actual sample temperature was approximately 0.5 K above this. The first structures were created by depositing Ge layers of varying thickness onto bulk Si, then capping these layers with Si to a depth of 200 Å:

Si	200 Å
Ge	5 to 20 monolayers (ML)
Si	bulk material (100) orientation

Fig. 4.5.4 shows the spectrum obtained for the 10 ML sample, and is characteristic for each of the samples observed. The spectra contain Si-related band edge features at energies between approximately 8500 and 9500 cm^{-1}, and a broad line with peak energy at approximately 6500 cm^{-1}.

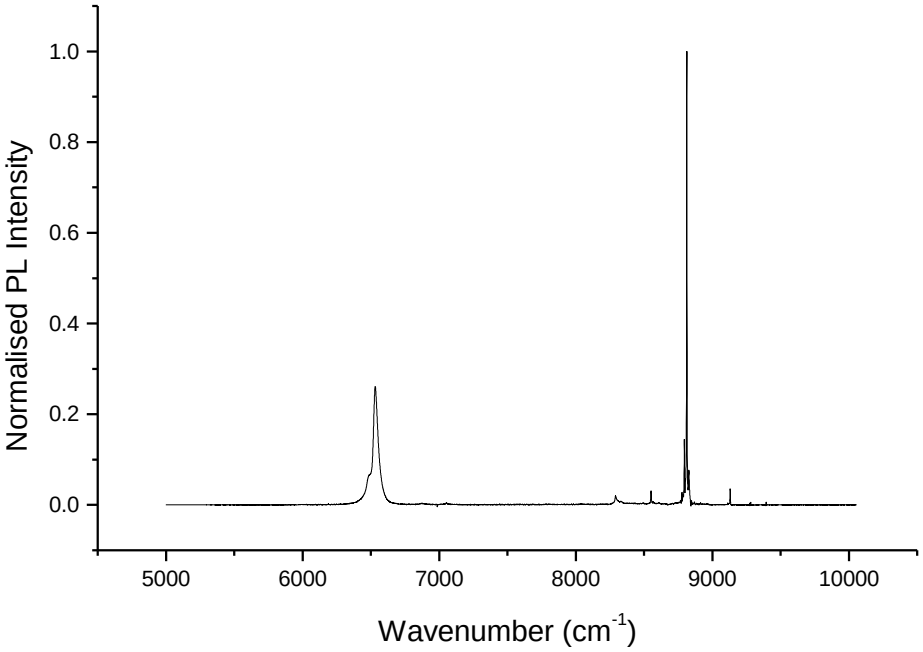

Fig. 4.5.4: Plot of PL intensity (normalised to BE) versus energy for 10ML sample, at 4.2 K. It shows the general spectral features of all samples examined

Fig. 4.5.5 is an enlargement of this broad feature. It is made up of two superimposed peaks, each of which is discussed below. The most intense peak will be referred to as the *major* feature, whilst the slightly weaker peak at lower energy will be referred to as the *minor* feature, manifesting itself as a kink on the broad tail. *Fig. 4.5.6* shows that the intensity ratio between these peaks is maintained for different monolayer thickness within the errors introduced by the normalisation process.

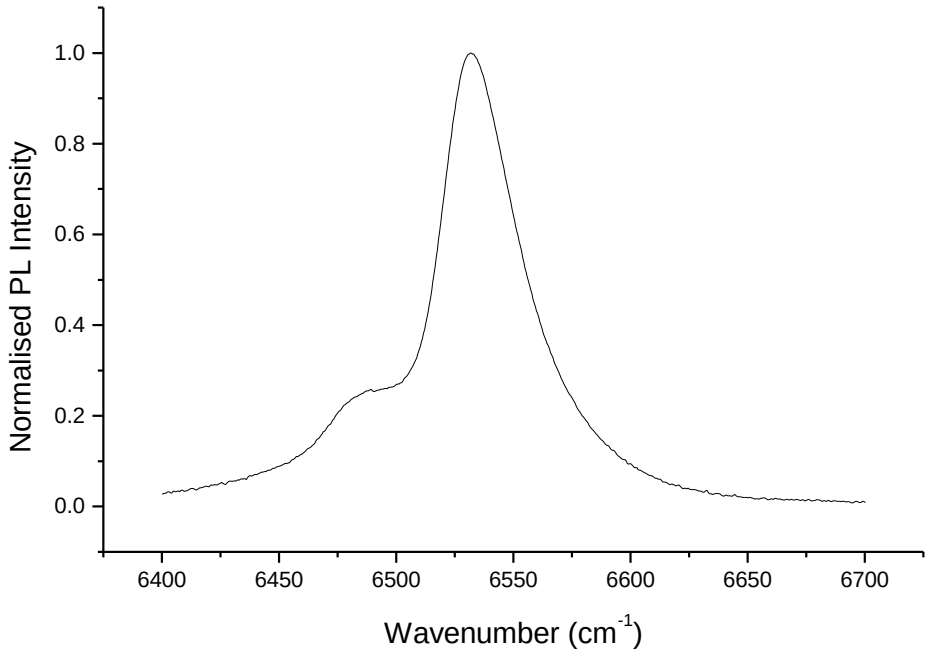

Fig. 4.5.5: Enlargement of the broad feature present in the 10ML sample. It is made up of two overlapping peaks – the lower energy peak appearing as a kink in the trailing tail of the major line. This line shape is characteristic of all samples examined

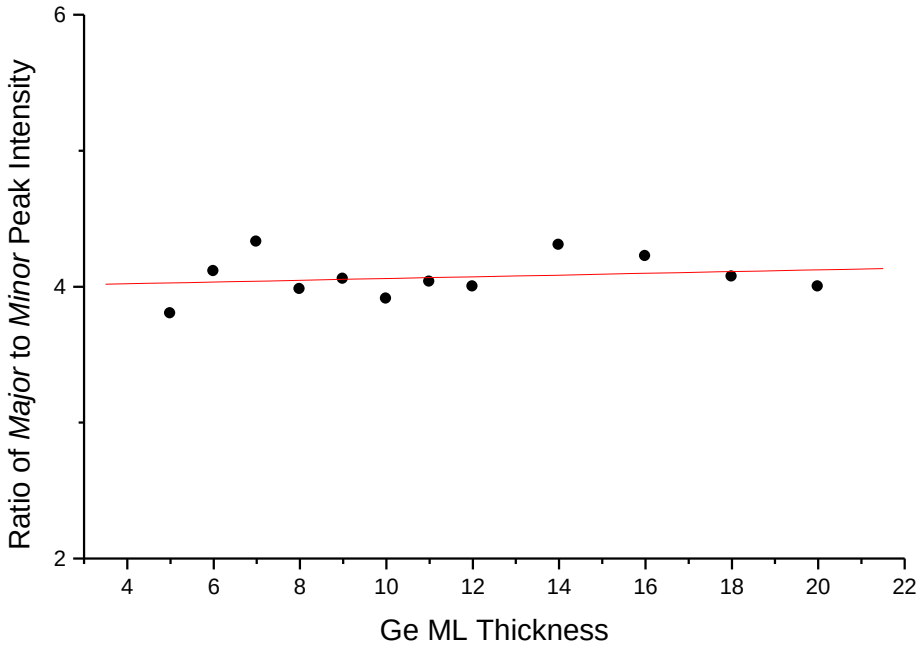

Fig. 4.5.6: Graph illustrating that the ratio of the intensities of the major and minor peaks remains relatively constant despite changes in monolayer thickness

Both the intensity and width of this peak, as functions of monolayer thickness, are shown in *Figs. 4.5.7* and *4.5.8* respectively. From these graphs it can be seen that maxima in both intensity and width occur around the 10 ML region and, since data for these graphs have been normalised, these phenomena are the result of intrinsic properties of the material and are not related to experimental variations.

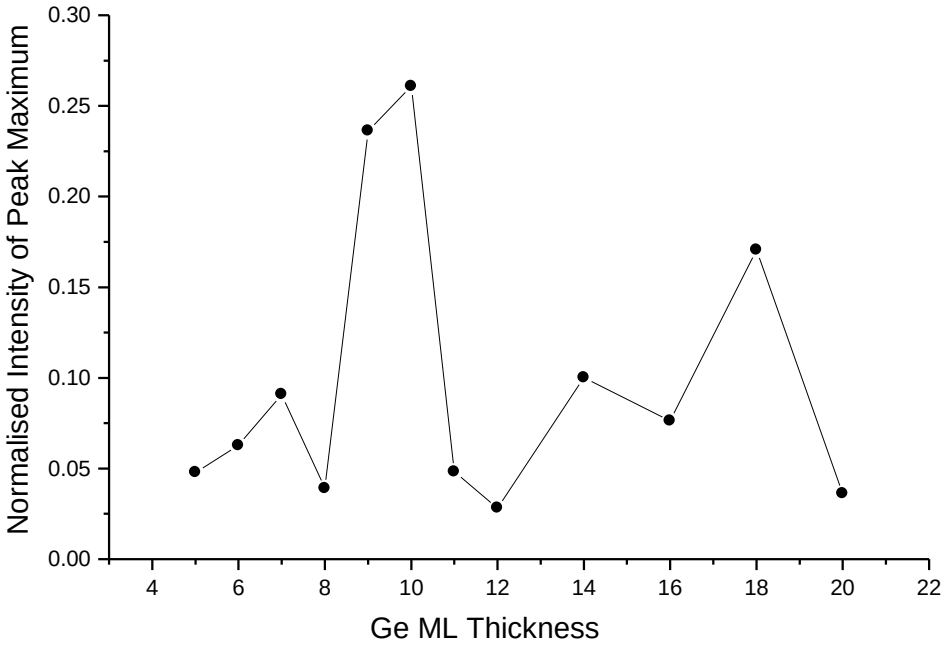

Fig. 4.5.7: Plot of PL intensity vs monolayer thickness, indicating maximum luminescence at 10 ML

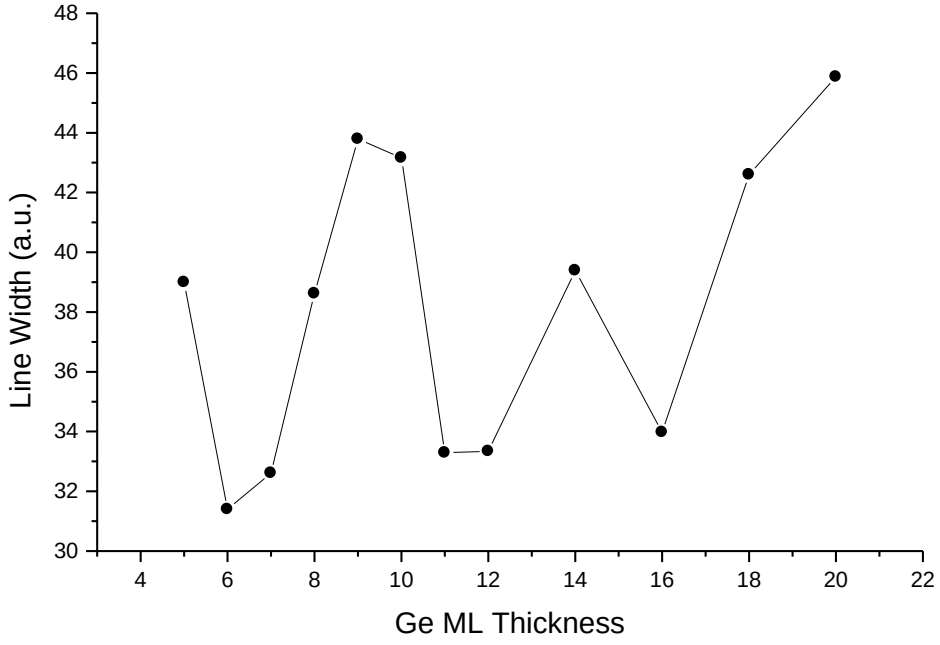

Fig. 4.5.8: Graph of line width versus monolayer thickness. The width is that of a Lorentzian fit to the major line, which is found to better approximate the broad tail than a standard Gaussian

Fig. 4.5.9 depicts the peak energy position of the major line as a function of monolayer thickness. It is found to have an average energy of 6529.0 cm^{-1} (809.6 meV), with a variation of approximately ± 3 cm^{-1} (0.37 meV) depending on the sample. From data not presented graphically here, the minor peak has an energy of approximately 6488 cm^{-1} (805 meV). Based on the energies of these two components, the general double-peak characteristic of the line shape, and the lack of correlation between the PL intensity and ML thickness, it is extremely likely that this broad feature is the *D1* dislocation line of Si.

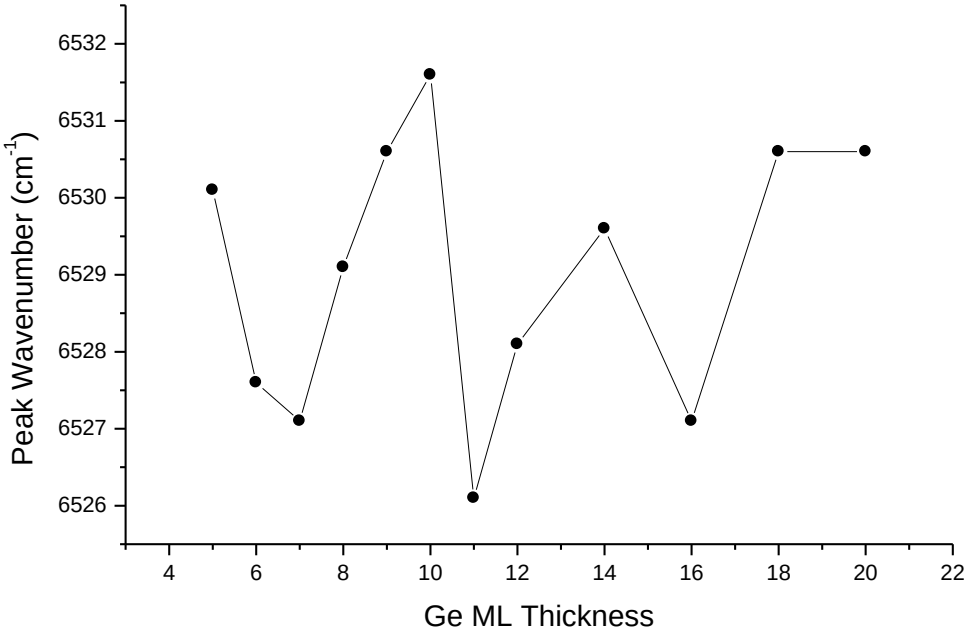

Fig. 4.5.9: Variation of peak energy position of the major feature with monolayer thickness

The *D1* dislocation feature is observed at an energy of 807 meV, according to G. Davies[2], close to the 809.6 meV energy of the feature discussed above. The slight energy difference is due to variations in the doping and impurity concentrations between samples, and the effects of slightly different strain conditions. *Fig. 4.5.10* is the PL spectrum of the *D1* feature when a Si sample was placed under stress, as obtained by Sauer *et al.*[3]. It shows a two-peak structure which correlates to the major and minor features described above, bearing in mind the minor peak in *Fig. 4.5.10* is shifted dramatically to lower energy as a result of the stress applied. Sauer *et al.* place the peak energy position of the *D1* line at 812 meV. The observed position of 809.6 meV for the major line in the Si:Ge samples, lying between the 807 and 812 meV quoted elsewhere, is therefore entirely consistent with the *D1* assignment.

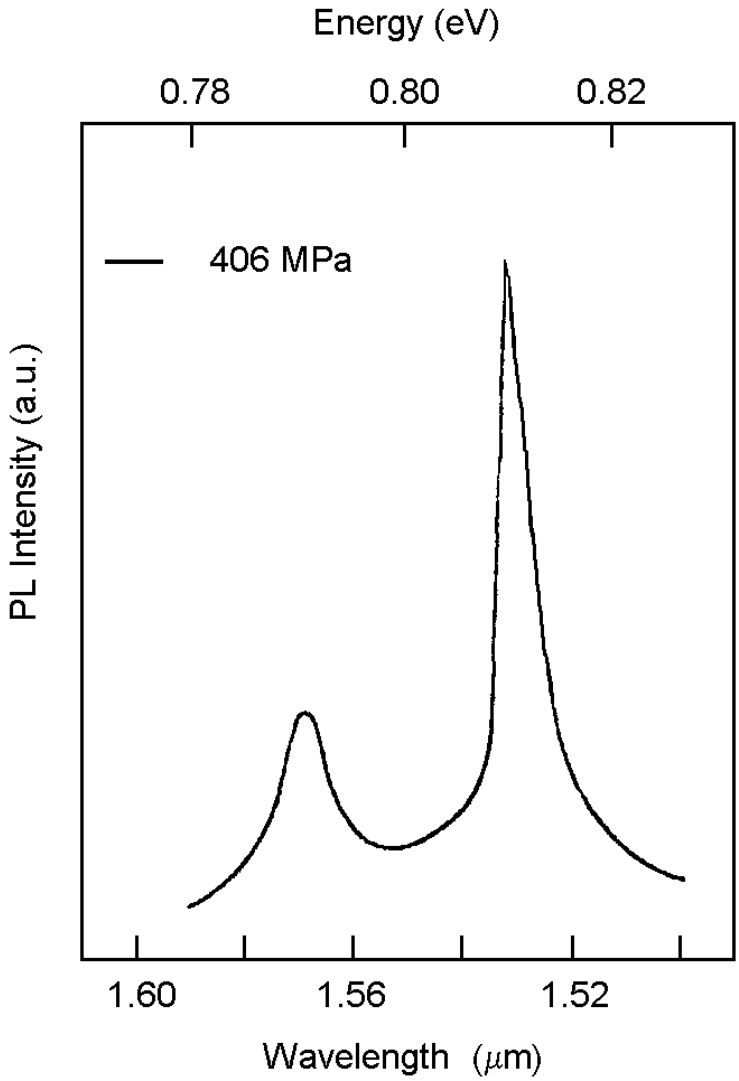

Fig. 4.5.10: The D1 dislocation line as observed by Sauer et al. after applied stress – the revealed double peak structure and peak energy position suggest it is the same feature as that observed in the discussed Si:Ge samples

The second sample type contained a more complicated structure:

Si	235Å
Si	20 Å
Ge	Thin layer deposited for 16 seconds
Si	100 Å
$Ge_{0.05}Si_{0.95}$	Layers containing 95% Si, 5% Ge
Si	1150 Å
Si	bulk material p-doped (B) (100) orientation

Fig. 4.5.11 shows the broad line as obtained for this sample as compared to the feature discussed previously for the sample containing 9ML Ge. The graph has been normalised so each appears the same intensity. Although there is a difference in line widths, the energy position of this line and the slightly asymmetric appearance of the low energy tail still suggest that it is also related to the *D1* dislocation line.

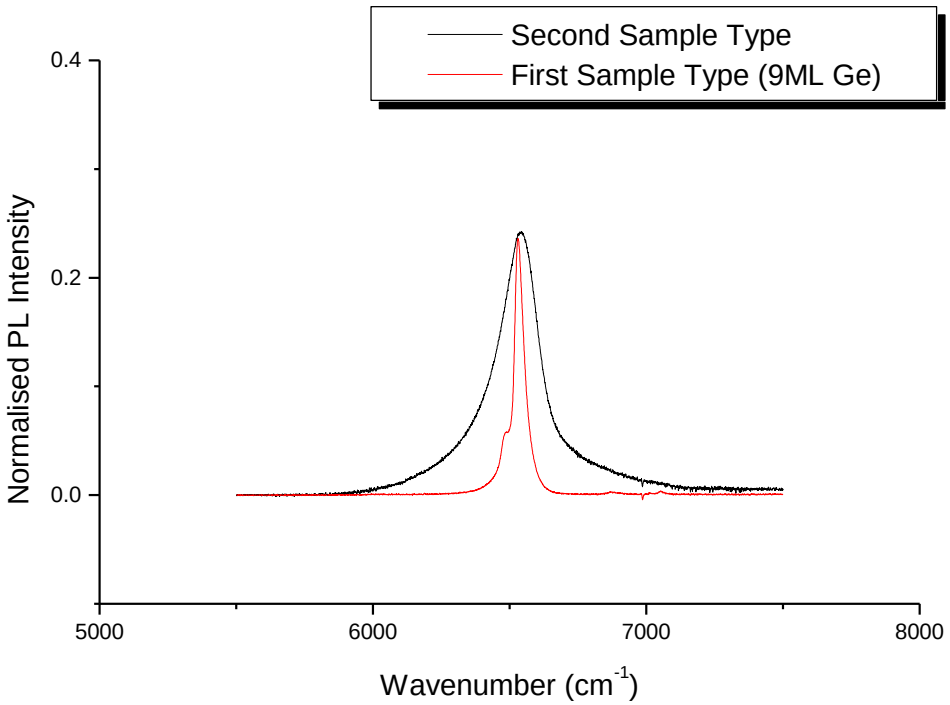

Fig. 4.5.11: Broad line observed in second sample type compared to line seen in the 9ML Ge sample of first type. The energy of lines is similar, suggesting the feature observed in the second sample type is also related to the D1 dislocation line of Si

Finally, the third sample type was a p-p^+-n^+ diode. A heavily doped n-type (n^+) region was created on a silicon p-type substrate with a heavily doped p-type surface (p^+). This arrangement is shown in *Fig. 4.5.12* along with the positions of connecting wires. Ge quantum wells lie between the bulk material and the doped surface. *Fig. 4.5.13* illustrates the single feature observed in the spectrum from this sample, excluding the Si band edge phenomena. The peak energy position of this single line is 6187.1 cm^{-1} (767.2 meV). Due to its narrow line width, it is thought to be the *P*-line (767.3 meV) which is a C-related centre produced by radiation damage and annealing at 450°C in CZ silicon[4,5].

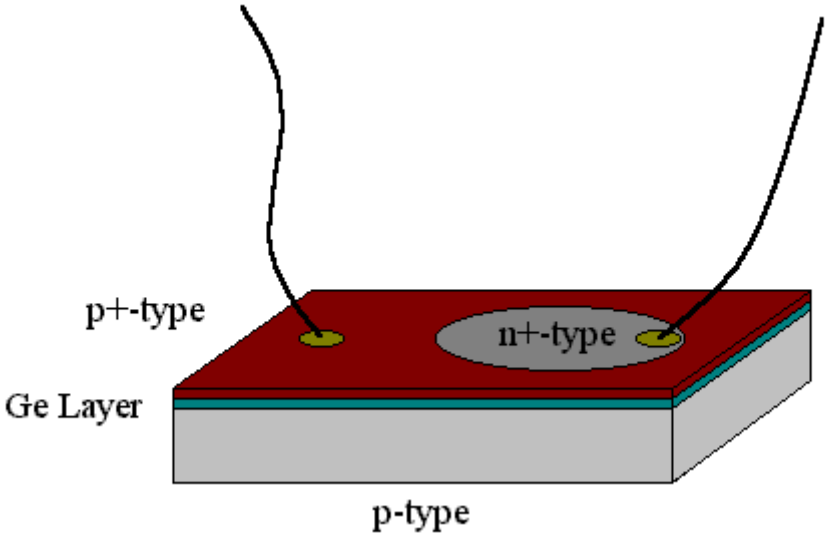

Fig. 4.5.12: The p-p^+-n^+ diode. Heavily-doped p- and n-type regions were layered onto bulk Si. Ge quantum structures are present between the electrical contacts beneath the thin surface-doped Si layers

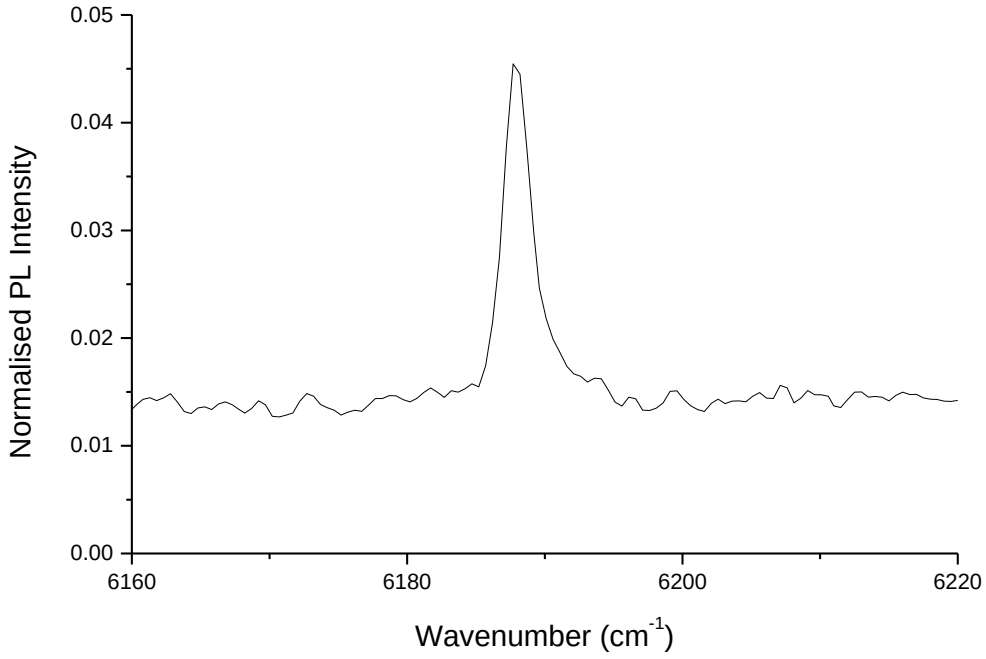

Fig. 4.5.15: Narrow line observed from diode sample. It is believed to be the Si P-line

From the above analysis, it seems likely that the luminescence observed from all samples was entirely unrelated to the Ge structures present. Either the growth of Ge introduces dislocations in the Si above the layer, or the quality of bulk Si was poor and dislocations were already present in this material. Based on the the PL data currently obtained, one cannot be confident which of these assessments is the correct one, although the use of a technique such as DLTS may be able to distinguish between surface and bulk defects.

Whilst evidence has been presented here that relates the features observed to the *D1* dislocation line for the first sample types, one cannot rule out the possibility that the observed luminescence is related to quantum wells, or that this luminescence is present but overwhelmed by the intensity of dislocation-related phenomena. There is a technique, however, that could establish the nature of the spectra observed with absolute certainty, but it involves gradual destruction of the material.

If an etch were performed that removed the capping layers of Si and the sample was then analysed, one would not expect to see dislocations related to those top layers. Should the defect remain, however, then a second etch could be used to destroy the Ge layers. Again, if the PL peak disappeared from the spectrum, it could be concluded that the feature was actually related to the Ge layers. If it was subsequently observed though, one could be certain that it was related to the bulk material**.** Since the majority of my work was in relation to Hg- and Au-related defects, there was insufficient time to investigate the nature of the MQW structures in greater detail than already described. The hypothetical etching technique described here is included as a possible reference for future work.

Section 5: Conclusions

Whilst the implantation of radioactive isotopes into semiconductors has been shown previously to be a powerful and relatively simple method of determining the chemical identity of defects, this research uncovers some major logistical problems that must be borne in mind when using the technique. Spectroscopic observations of samples must begin shortly after implantation, within the constraints placed by radiation safety considerations. Choosing longer-lived isotopes in the hope that sufficient material will remain after lengthy transport to spectroscopic equipment has not proven to be a viable alternative. There have not only been problems associated with the subsequent low concentration of defects due to decay over time, but also difficulties due to thermal dissociation of defects as a result of storage at room temperature. In the case of the 'FeB' defect, it has been shown that a period of a few days is sufficient to introduce significant errors to the data one might obtain. Since the high activity of samples will result in a delay at radioactive ion implantation facilities, and it will generally take time for the issuing of export licenses, etc, spectroscopic equipment should ideally be located on-site. In short, the dilemma the experimenter faces is this - if one implants short-lived isotopes, then equipment needs to be nearby. If one implants long-lived isotopes, then samples must not be allowed to sit at room temperature for extended periods of time. This places severe limitations on the type of experiments that can be realistically carried out.

As yet it has not been determined if it is preferable to anneal Hg-implanted samples before or after shipment. Whilst we know that the Hg is driven towards the surface of the material during the anneal, and can be released from the samples at temperatures of about 1000 °C, the behaviour of end products of the decay (Au, Pt, Ir, Os, or W depending on the isotope of Hg used) must also be considered. The best way of determining if there is any significant difference in PL spectra and defect concentration, depending on when the samples are annealed, is to investigate it experimentally.

Using the decay of ^{197}Hg, and demonstrating that phonon energies are consistent with high-mass transition metals, there is strong evidence that the broad feature found in Hg-implanted Si is related to Hg. The use of stable ^{200}Hg has proven valuable in enabling a more detailed examination of the defect. The band contains three Zero Phonon Lines located at 780.4, 783.1, and 785.5 meV.

On the basis of temperature dependency data, the results suggests that this Hg defect has two excited states, with an energy separation of 0.7 meV between them, and three ground states. The results presented show that the band probably contains at least two systems of Stokes lines (and possibly more), related to these ZPLs. Based on an analysis of this sideband, the Huang-Rhys factor with respect to ZPL Hg_0 is 1.4 and the relaxation energy is 8.1 meV. The corresponding values in relation to ZPL Hg_1 are 2.6 and 14.8 meV. Further work will be required to verify the energy level scheme proposed.

Implantations using radioactive Hg ions will be necessary to identify the unusual band, labelled '*x*' here, which appears to have at least one ZPL (831.8 meV) and a phonon separation of 4.8 meV. Since this feature has not been reported previously, it is tentatively suggested that it is related to atoms introduced by the implantation equipment rather than impurities present in the starting material. This would limit the identification of the defect to being Hg- or Au-related. Currently there is no evidence of the appearance of the defect in n-type material although this must be checked thoroughly, particularly now the upper-limit of temperature required to observe the defect is known. The feature vanishes from the spectrum at approximately 4.8 K, which could be the result of the defect existing in two different configurations. As the temperature approaches 5 K, the second configuration dominates. If this second state was not optically active, it might explain the results observed. In any case, more work is required to identify this defect.

With respect to the 'FeB' defect observed at 1067 meV, whilst the data presented here does not corroborate the previous Au identification, it does add weight to this assessment. Despite experimental evidence that the line could be Hg-related, thermal dissociation has been offered as an explanation which is not only consistent with previously established behaviour, but does not require one to re-evaluate the Au assignment. A repetition of this experiment is necessary to confirm that the feature is Au-related, but I have shown it is essential that such observations begin shortly after implantation for this particular defect.

Again, whilst data here cannot verify the identity of the 1004 meV AuLi defect directly it does seem increasingly likely, on the basis of this research, that this assignment is the correct one. Since the defect has only been reported in the case of Hg being implanted into silicon, and only appears in those samples diffused with Li, it is plausible that the defect is created as a complex containing Hg and Li, only becoming radiative as the Hg decays to Au. It has not been observed in

more than twenty Hg implanted samples that were not diffused with Li. The data presented here is, albeit indirect, proof of the involvement of both Hg and Li. Further study will be necessary to investigate if migration of Au from the defect is the cause of the unusual data for the decay rate. Since the decay data could be fit to 70 hours, and this rate is similar to that for the 'FeB', it seems very likely that the behaviour of Au in these complexes is similar.

Finally, the PL of Si:Ge quantum structures did not reveal any evidence of luminescence related to the wells themselves. The dominance of dislocation-related features in the spectra is conclusive testimony to the necessity of very pure silicon for the growth of these structures, and is an indication of the difficulty in producing heterojunctions with such lattice-mismatched materials. Whilst strained-layers do offer significant technical applications, the use of PL to examine such structures is fraught with the type of dislocation-related problems illustrated here. PL, in this standard form, is incapable of determining whether defects are surface or bulk material related. In relation to layered samples the usefulness of the technique is questionable. It could provide valuable information if measurements were made before and after each layer of material is laid down. This is the reason I have suggested a destructive etching process to determine the actual location of dislocation-related luminescence, and/or the degree to which the Ge layer affects the spectrum of the samples. Other techniques, in particular DLTS, are more suited to investigations of this type, and surface probing methods, such as STM or AFM, could provide valuable information if the strained layers are examined after plasma deposition.

Section 6: References by Section

Section 1: Introduction

1. H. Bender and J. Vanhellemont, *Handbook on Semiconductors*, (North-Holland, Amsterdam), **3B**, 1637 (1994)

2. J. A. Baker, T. N. Tucker, N. E. Moyer and R. C. Buchert, J. Appl. Phys., **39**, 4365 (1986)

3. J. Weber, R. J. Davis, H. U. Habermeir, W. D. Sawyer and M. Singh, Appl. Phys. A, **41**, 175 (1986)

4. J. R. Noonan, C. G. Kirkpatrick and B. G. Streetman, J. Appl. Phys., **47**, 3010 (1976)

5. A. R. Bean and R. C. Newman, J. Phys. Chem. Solids, **30**, 1493 (1969)

6. C. E. Jones, D. Schafer, W. Scott and R. J. Hager, J. Appl. Phys., **52**, 5148 (1981)

7. E. McGlynn, M. O. Henry and P. McLoughlin, Phys. Rev. B, **59**, (15), 10 084 (1999)

8. A. C. T Drakeford and E. C. Lightowlers, Mater. Res. Soc. Symp. Proc., **59**, 209 (1988)

9. S. E. Daly, M. O. Henry, K. G. McGuigan and M. C. doCarmo, Semicond. Sci. Technol., **11**, 996 (1996)

10. M. O. Henry, J. D. Champion, K. G. McGuigan, E. C. Lightowlers, M. C. doCarmo and M. H. Nazzare, Semicond. Sci. Technol., **9**, 1375 (1994)

11. E. McGlynn, M. O. Henry, K. G. McGuigan and M. C. doCarmo, Phys. Rev. B, **54**, (20), 14 494 (1996)

12. M. O. Henry, S. E. Daly, K. Freitag and R. Vianden, J. Phys. Condens. Matter, **6**, L643 (1994)

13. R. Magerle, A. Burchand, M. Deicher, T. Karle, W. Pfeifferr and E. Rechnagel, Phys. Rev. Lett., **75**, 1594 (1994)

Section 2: Photoluminescence Spectroscopy

1. P. K. Basu, *Theory of Optical Processes in Semiconductors (Bulk and Microstructures)*, (Oxford Science Pub.), Ch. 10, pp. 205-233 (1997)

2. G. Davies, Physics Reports, (North-Holland, Amsterdam), **176**, (3 & 4), 83 (1989)

3. A. N. Safonov, E. C. Lightowlers, Mat. Sci. Eng. B, **58**, 39 (1999)

4. E. C. Lightowlers, *Growth and Characterisation of Semiconductors*, (Adam Hilger, Bristol), Ch. 5, (1990)

5. P. McLColley and E. C. Lightowlers, Semicond. Sci, Technol., **2**, 157 (1987)

Section 3: Sample Preparation, Implantation, and Annealing

1. E. Kugler, D. Flander, B. Jonson, H. Haas, A. Przewloka, H. L. Ravn, D. J. Simon, K. Zimmer and the ISOLDE Collaboration, *The New CERN-ISOLDE On-Line Mass-Separator Facility At The PS Booster*, European Organisation For Nuclear Research, **CERN-PPE/91-170**, (1991)

2. E. Hagebø, P. Hoff, O. C. Jonsson, E. Kugler, J. P. Omtvedt, H. L. Ravn and K. Steffensen, *New Production Systems At ISOLDE*, European Organisation For Nuclear Research, **CERN-PPE/91-179**, (1991)

Both above papers can also be found in the *Proceedings of the 12th International Conference on Electromagnetic Isotope Separators and Techniques Related to Their Application*, Sendai, Japan, September 2-6, 1991

3. The ISOLDE Website can be found at: http://isolde.cern.ch/ISOLDE

4. H. J. Kluge, *ISOLDE Users' Guide*, European Organisation For Nuclear Research, **CERN 86-05**, Experimental Physics Division, July 18th (1986)

5. A. Henry, B. Monemar, J. P. Bergman, J. L. Lindström, P. O. Holtz, Y. Zhang and J. W. Corbett, Phys. Rev. B, **47**, (20), 13 309 (1993)

6. K.-M. Wang, B.-R. Shi, S.-J. Ma, H.-Y. Zhai, X.-D. Liu, J.-T. Liu and X.-J. Liu, J. Appl. Phys. **74**, 2306 (1993)

Section 4.2: Hg-Related Defect

1. M. O. Henry, E. McGlynn, J. Fryar, S. Linder and J. Bollmann, Nucl. Instr. and Meth. in Phys. Res. B, **178**, 256 (2001)

2. M. O. Henry *et al.*, Proc. 23rd ICPS, (World Scientific Publ. Co., Singapore), 2713 (1996)

3. M. O. Henry, E. Alves, J. Bollmann, A. Burchard, M. Deicher, M. Franculli, D. Forkel-Wirth, M. H. Knopf, S. Linder, R. Magerle, E. McGlynn, K. G. McGuigan, J. C. Solares, S. Stötzler and G. Weyer, Phys. Stat. Sol. (b), **210**, 853 (1998)

4. S. Linder, Thesis for the award of MSc, Dublin City University (1999)

5. H. Conzelmann, Appl. Phys. A, **42**, 1 (1987)

6. S. P Watkins, M. L. W. Thewalt and T. Steiner, Phys. Rev. B, **29**, (10), 5727 (1984)

Section 4.3: 'FeB'-Related Defect:

1. G. W. Ludwig and H. H. Woodbury, Sol. Stat. Phys., **13**, 223 (1962)

2. R. Sauer and J. Weber, Physica, **116B**, 195 (1983)

3. K. Graff and H. Pieper, J. Electrochem. Soc., **128**, 609 (1981)

4. H. D. Mohring, J. Weber and R. Sauer, Phys. Rev. B, **30**, (2), 894, (1984)

5. T E. Schlesinger, R. J. Hauenstein, R. M. Feenstra and T. C. McGill, Solid State Commun., **46**, 321 (1983)

6. J. Klugge, W. Gehlhoff and J. Donecker, Acta Phys. Polon. A, **73**, 207 (1988)

7. M. O. Henry, M. Deicher, R. Magerle, E. McGlynn and A. Stotzler, Hyper. Int., **129**, 443 (2000)

8. M. O. Henry, E. Alves, J. Bollmann, A. Burchard, M. Deicher, M. Franculli, D. Forkel-Wirth, M. H. Knopf, S. Linder, R. Magerle, E. McGlynn, K. G. McGuigan, J. C. Solares, S. Stötzler and G. Weyer, Phys. Stat. Sol. (b), **210**, 853 (1998)

Section 4.4: AuLi-Related Defect

1. M. O. Henry, E. McGlynn, J. Fryar, S. Linder and J. Bollmann, Nucl. Instr. and Meth. in Phys. Res. B, **178**, 256 (2001)

2. A. Henry, B. Monemar, J. P. Bergman, J. L. Lindstrom, P. O. Holtz, Y. Zhang and J. W. Corbett, Phys. Rev. B, **47**, (20), 13 309 (1993)

Section 4.5: Si:Ge Quantum Well Structures

1. L. Pavesi and M. Guzzi, J. Appl. Phys., **75**, 4782 (1994)

2. G. Davies, Physics Reports, (North-Holland, Amsterdam), **176**, (3 & 4), 83 (1989)

3. R. Sauer, J. Weber and J. Stolz, Appl. Phys. A, **36**, 1 (1985)

4. J. Wagner, A. Dornen and R. Sauer, Phys. Rev. B, **31**, (8), 5561 (1985)

5. G. Davies, E. C. Lightowlers, R. A. Woolley, R. C. Newman and A. S. Oates, J. Phys. C, **17**, L499, (1984)